The EUMETSAT Network of Satellite Application Facilities

ROM SAF
Radio Occultation Meteorology

ROM SAF CDOP-2

Visiting Scientist Report 31:

Radiosonde Temperature Bias Corrections using Radio Occultation Bending Angles as Reference

Jordis S. Tradowsky

Danish Meteorological Institute (DMI)
European Centre for Medium-Range Weather Forecasts (ECMWF)
Institut d'Estudis Espacials de Catalunya (IEEC)
Met Office (METO)

Ref: SAF/ROM/DMI/REP/VS/31
Issue: Version 1.1
Date: 30th June 2017

DOCUMENT AUTHOR TABLE

	Author(s)	*Function*	*Date*	*Comment*
Prepared by:	Jordis Tradowsky	ROM SAF Visiting Scientist	9th Dec 2016	
Reviewed by (Internal):	Chris Burrows	ROM SAF Project Team	15th Dec 2016	
Approved by:	Kent B. Lauritsen	ROM SAF Project Manager	30th June 2017	

DOCUMENT CHANGE RECORD

Issue/Revision	*Date*	*By*	*Description*
Version 0.1	9th Nov 2016	JT	First version
Version 0.2	16th Dec 2016	JT	Implemented CBs suggestions
Version 1	16th Dec 2016	JT	Implemented KBLs suggestions
Version 1.1	30th June 2017	JT	Updated the GRUAN analysis with a more detailed discussion of consistency and agreement between the departure statistics. Updated Fig.5.2. Updated the uncertainty bars in Figs.6.8, 6.11, 6.14, 6.17, and 6.23. Added a citation to the recently published paper Tradowsky et al. (2017) explaining the method applied here. Including comments from Greg Bodeker on chapter 6.

VS Authors
This VS study was carried out by Jordis Tradowsky, Bodeker Scientific, New Zealand; email: jordistradowsky@gmail.com

VS Duration
The VS study was performed during August - October 2016 at the Met Office with one short visit to ECMWF.

ROM SAF

The Radio Occultation Meteorology Satellite Application Facility (ROM SAF) is a decentralised processing center under EUMETSAT which is responsible for operational processing of GRAS radio occultation data from the Metop satellites and Radio Occultation (RO) data from other missions. The ROM SAF delivers bending angle, refractivity, temperature, pressure, and humidity profiles in near-real time and offline for NWP and climate users. The offline profiles are further processed into climate products consisting of gridded monthly zonal means of bending angle, refractivity, temperature, humidity, and geopotential heights together with error descriptions.

The ROM SAF also maintains the Radio Occultation Processing Package (ROPP) which contains software modules that will aid users wishing to process, quality-control and assimilate radio occultation data from any radio occultation mission into NWP and other models.

The ROM SAF Leading Entity is the Danish Meteorological Institute (DMI), with Cooperating Entities: i) European Centre for Medium-Range Weather Forecasts (ECMWF) in Reading, United Kingdom, ii) Institut D'Estudis Espacials de Catalunya (IEEC) in Barcelona, Spain, and iii) Met Office in Exeter, United Kingdom. To get access to our products or to read more about the ROM SAF please go to: http://www.romsaf.org.

Intellectual Property Rights

List of Contents

Executive Summary

For the purpose of numerical weather prediction (NWP), both radio occultation (RO) and radiosonde (RS) measurements are used to anchor the temperature. Thus, it is important to try to eliminate biases between these two observation types prior to the assimilation into the numerical weather forecast. Following the development of a new method to estimate corrections for stratospheric RS temperature biases using RO bending angles as an unbiased reference as presented in ROM SAF VS26 (Tradowsky [35]), this study focuses on three work packages.

1. Station-by-station temperature bias corrections to be applied in a forecast impact study using the Met Office global numerical weather prediction system are calculated for 852 upper-air stations. While the stratospheric correction is calculated using a double differencing approach of RS and RO background departures, smoothing towards the default correction is done in the troposphere, where RS biases are generally smaller.
2. Rather than using statistical optimization of high level BAs as is done in the conventional RO retrieval, the method applied here (see Tradowsky [35]) applies a cut-off impact height above which all BA departures are set to zero before they are propagated into dry temperature (Tdry) departures using a linear operator. The cut-off is applied for two purposes, (i) to eliminate the effect of noisy high level BAs and (ii) to enable the use of double differencing, which relies on the assumption of a constant model bias over the separation distance of the RO and RS measurements — hence, including model background information up to a significantly higher level in the RO departures than in the RS departures would invalidate this central assumption. While the cut-off is therefore needed in this project, it also adds structural uncertainty to the derived Tdry departures, similar to the way in which choosing an implementation of statistical optimization would add structural uncertainty. The structural uncertainty is calculated and discussed in the third part of this report.
3. The reference-quality RS data product from the Global Climate Observing System (GCOS) Reference Upper-Air Network is compared with RO using their respective background departures in the stratosphere. As the RO technique and the GRUAN data product both offer high quality data products, good agreement is expected.

The bias correction profiles calculated here are prepared for a forecast impact study to be performed at the Met Office and include corrections for four different solar elevation angle (SEA) ranges. If the sample size within a SEA range is too small to calculate a correction, SEA ranges are combined and it is shown that this is a suitable estimate of the bias correction for the majority of sites.

This report also discusses how the tangent linear retrieval which is used to calculate the Tdry departures from BA departures compares to other RO retrievals. While optimization of high level BAs with a smooth *a priori* profile is used in the conventional retrieval, here we explicitly set the high level BA departures to zero and calculate the Tdry departures from a subset of BA departures. This is essential in order to use a NWP model as the transfer medium in the comparison of two measurement techniques. It is shown that cutting off high level BA departures indeed gives similar results to applying a simplified algorithm that approximates the results that would be obtained using statistical optimization.

The comparison of GRUAN temperature departures with RO Tdry departures illustrates another usage of the technique. For most GRUAN sites, good agreement between RO and GRUAN is found at most levels, but the highest level, the GRUAN temperatures are warmer than RO Tdry. However the GRUAN temperatures are colder than RO Tdry at most levels at the station Southern Great Plains, which will require further investigation.

1 Introduction

For decades, radiosonde (RS) profiles have been assimilated into numerical weather prediction (NWP) systems and, since 2006, radio occultation (RO) data have been assimilated, demonstrating a positive impact on weather forecasts (see Healy [17], Poli et al. [27], Rennie [28]). However, the impact of the high quality RO data may be limited by opposing biases between the observation types. Furthermore, local and regional variations in RS temperature biases have the potential to cause false horizontal temperature gradients in NWP analyses, which would lead to spurious features in the wind field. Satellite radiance measurements require bias corrections when assimilated into NWP models, and these corrections are computed relative to the model background or analysis, either statically (Eyre [10], Harris and Kelly [14]), or via variational methods (Derber and Wu [8], Dee [7], Auligné et al. [3]). This can only be done consistently if sufficient “anchor" measurements are present in the assimilation system. Amongst these, RO and RS are key contributors and thus, ensuring consistency between the bias characteristics of these observation types is important for the stability of the assimilation systems.
The ROM SAF Visiting Scientist Report Report 26 (Tradowsky [35]) described a new technique to calculate RS temperature biases in the stratosphere, using RO bending angles as the reference. Instead of using co-locations, the Met Office Unified Model is used as a transfer medium. The difference between the background departures of RO and RS estimates the RS temperature bias, under the assumptions that the RO observations are unbiased and that the model background cancels out when the differencing is performed. For this purpose the RO BA departures are propagated into dry temperature (Tdry) departures using a tangent linear Tdry retrieval, which, rather than using statistical optimization, calculates the Tdry departures from a subset of the BA departures. This is achieved by setting the BA departures above an impact height of 35 km to zero. This method allows to control the flow of information better than using statistical optimization, and it is shown, that the applied cut-off gives results similar to smoothing the BAs with a climatological value as it is done in the conventional (non-linear) Tdry retrieval chain.

This ROM SAF visiting scientist project comprises three major objectives:

1. The preparation of temperature bias correction to be applied in a forecast impact study,
2. The analysis of radiosonde reference temperature profiles from the GCOS[1] Reference Upper-Air Network, and
3. The estimation of structural uncertainty added by choosing a cut-off impact height as discussed in Tradowsky [35].

While the method to calculate stratospheric temperature bias corrections was developed in Tradowsky [35] and bias corrections were calculated for those solar elevation angle (SEA) ranges that have a sufficient measurements available, the provided bias corrections were not ready to be applied into NWP models. Thus, within this study a ‘best estimate’ of the bias correction to be applied in a forecast impact study is developed, which is based on bias corrections calculated using the method described in Tradowsky [35]. In Tradowsky [35] the stratospheric RS temperature bias was calculated for four solar elevation angle ranges, i.e. ‘high’, ‘low’, ‘dusk’, and ‘night’. For the preparation of a forecast impact study, inter alia, the

[1] Global Climate Observing System

statistics for different SEA ranges are combined in cases where insufficient measurements are available in one SEA range (see section 4.2.1). Furthermore the bias corrections are smoothed to a constant value of 0.1 K below the lowest available bias correction (see section 4.1) and if the standard error of the bias correction is large, a minimal bias correction is calculated and applied, see section 4.3.1.

The method developed in Tradowsky [35] can furthermore be used to compare model departures of the GCOS Reference Upper-Air Network Vaisala RS92 data product to the RO BA departures propagated into Tdry space. RO measurements (Ho et al. [18],Steiner et al. [32]), as well as GRUAN data product are known to be of reference quality (see Dirksen et al. [9]) and thus a good agreement between the two datasets, taking into account the uncertainties, is expected.

In the third work package (see chapter 5), an estimate of the structural uncertainty that is added by choosing a cut-off impact height is calculated. As every assumption that is made within a retrieval, deciding for an impact height above which the BA departures are set to zero, is adding structural uncertainty.

This report begins by giving a brief summary of the method used in chapter 2, continues by describing the RS and RO data sets in chapter 3, followed by a description of the preparation of the forecast impact study in chapter 4, an analysis of the GRUAN data in chapter 6 and an estimation of the structural uncertainty in chapter 5. The results are summarized and discussed in chapter 7.

2 Method

The RS temperature bias corrections are calculated on a station-by-station basis, giving a vertical bias correction profile for 852 upper-air stations that were assimilated in the Met Office global numerical weather prediction (NWP) system in 2015. A double-differencing approach, using the Met Office global NWP system as a transfer medium is applied to the mean RS temperature departures and the mean RO Tdry departures. For every RS profile at a given station, the departure from the model background (short-range forecast) is calculated on standard pressure levels[1] used in the alphanumeric TEMP format (Ingleby and Edwards [20]). Then, the mean RS temperature departure (observation minus background, i.e. O-B) is calculated. The RO BA departure is calculated using all COSMIC RO profiles measured within a circle with a radius of 500 km around the upper-air site. The RO BA is used rather than a retrieval of the temperature as it is a comparably raw variable, which does not include substantial *a priori* information. This is also one of the reasons why most NWP centres assimilate RO BAs . A tangent linear retrieval as described in Tradowsky [35] is used to propagate the BA departures to Tdry departures within this project. RO Tdry provides a valid estimate of the physical temperature only at levels of the atmosphere where water vapour is negligible and thus the Tdry departures are calculated in the stratosphere only. The lowest dry level is calculated from the model humidity individually for every RO profile allowing the use of RO measurements as low in the atmosphere as is reasonable for a given station.

The RS temperature bias correction is calculated as the difference between the mean RO Tdry departures and RS temperature departures, as

$$\overline{O_{RO} - O_{RS}} \simeq \overline{O_{RO} - B_{RO}} - \overline{O_{RS} - B_{RS}} \tag{2.1}$$

where O is the observation and B is the background, forward-modelled into observation space. The $\simeq$ denotes that the assumption has been made that B_{RO} and B_{RS} are equally representative of the true values at the RO and RS locations respectively, i.e the central assumption is that the NWP forecast bias does not vary between the RO and RS locations. This is a more robust assumption compared to direct co-locations between measurements, which are made assuming that the atmosphere does not vary over the separation distance. A similar double differencing approach is used by [12] to homogenize radiosonde temperature records.

A detailed description of the method, including the RO retrieval chain and a sensitivity study can be found in Tradowsky [35]. Furthermore a paper describing the method and chosen results is submitted to the *American Meteorological Society Journal of Applied Meteorology and Climatology*.

[1] 1000 hPa, 925 hPa, 850 hPa, 700 hPa, 500 hPa, 400 hPa, 300 hPa, 250 hPa, 200 hPa, 150 hPa, 100 hPa, 70 hPa, 50 hPa, 30 hPa, 20 hPa and 10 hPa

3 Data and Model

This study uses three different data sets and in addition short-range forecasts from the Met Office Unified Model is used to calculate the departures, i.e. the NWP system serves as a transfer medium. A detailed description of GRUAN and the currently available RS92 version 2 data set is given in section 3.1, followed by a short description of the COSMIC RO data, the RS data and the Met Office NWP system.

3.1 The GCOS (Global Climate Observing System) Reference Upper-Air Network

The GCOS Reference Upper-Air Network (GRUAN; www.gruan.org) was established to fill a long-recognized need of the international climate research community for reference quality measurements of upper-air essential climate variables. GRUAN was established following a series of meetings held jointly by GCOS and the United States National Oceanic and Atmospheric Administration (NOAA) between 2005 and 2007. As detailed in GCOS-112 [11], the purpose of GRUAN is to: 1. Provide long-term high quality climate records; 2. Constrain and calibrate data from more spatially-comprehensive global observing systems (including satellites and current radiosonde networks); and 3. Fully characterize the properties of the atmospheric column.
GRUAN currently comprises 24 sites (see Fig.3.1) that measure vertical profiles of essential climate variables such as temperature, pressure, and water vapour. These measurements are reference quality measurements in that all systematic biases have been accounted for and measurement uncertainties are provided as part of the GRUAN data products and these are traceable to internationally recognized measurement standards (Immler et al. [19]). Currently a GRUAN data product for the Vaisala RS92 is available, but data products for other RS, ozonesondes, frost point hygrometer, lidar, microwave radiometer and the Global Navigation Satellite System (GNSS) precipitable water vapour are under development. While GRUAN is not meant to provide a good spatial resolution of stations, the reference quality data products from the GRUAN stations are provided free of charge to the research community and can be used for a variety of studies. Bodeker et al. [5] gives an overview of the developments of GRUAN from the planning to the current network design.

Within this project the Vaisala RS92 GRUAN data product version 2 will be analysed for the years 2014 and 2015. As for the operational RS profiles, the departures from the model background are calculated on standard pressure levels and subsequently the GRUAN departures are compared with the RO departures. Some of the GRUAN stations also serve as operational upper-air sites, which means that the vendor supplied radiosonde product for the same launch is provided to the Global Telecommunication System (GTS). This would allow the measurements made at a GRUAN site (not the GRUAN data product which is not available in near-real time) to be assimilated into NWP models. Currently, effort within the GRUAN community is ongoing to receive a WMO station ID for all GRUAN sites and to enable all sites of the network to submit data to the GTS. Table 3.1 gives an overview of all GRUAN sites that provide a Vaisala RS92 product. Where available the WMO station IDs is included in the table.

For 14 of the sites shown in Fig. 3.1 a Vaisala RS92 GRUAN data product is available for at least parts of the years 2014 and 2015 (see table 3.1 for station details and number of

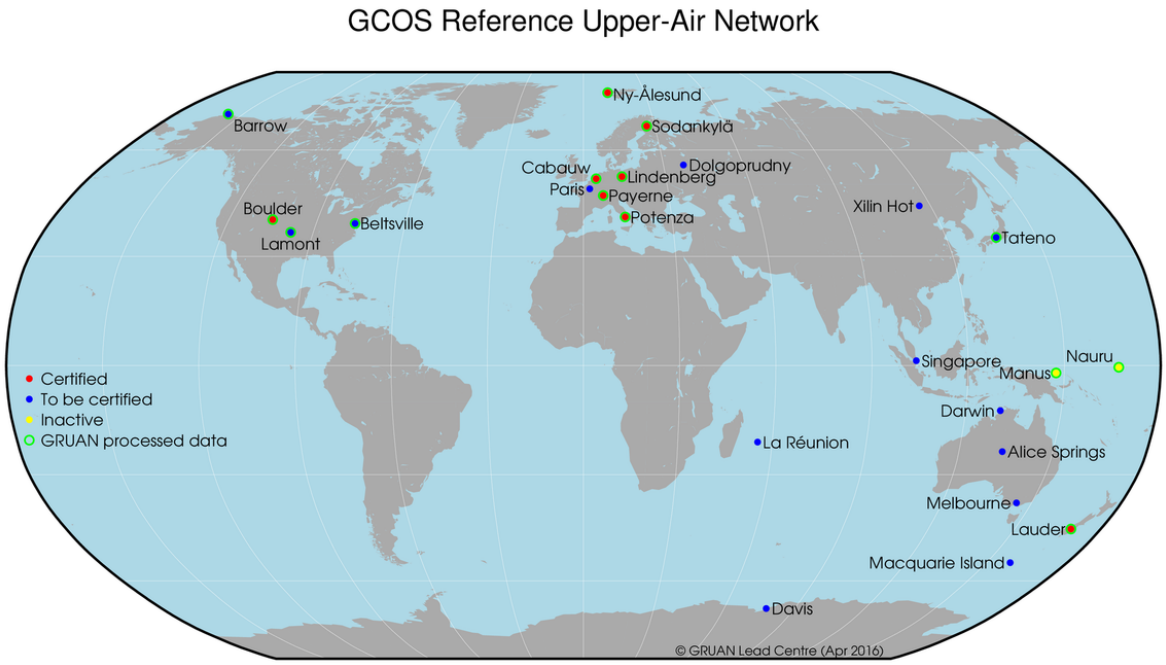

Figure 3.1: *Upper-air sites that contribute to GRUAN. Courtesy GRUAN Lead centre, figure from* `http://www.dwd.de/EN/research/international_programme/gruan/sites.html`

available profiles within 2014-2015). Version 2 of this GRUAN data product for the Vaisala RS92 will be analysed in this report, though it would be possible to repeat the analysis with the version 3, which is scheduled to become available late 2016/early 2017. Outliers in the GRUAN departures are rejected based on the Median Absolute Deviation (MAD) criterion as described in Tradowsky [35]. For the GRUAN sites Ny Ålesund (NYA), Sodankylä, Lindenberg, Cabauw, Barrow and Southern Great Plains (bold in table 3.1) sufficient profiles for the calculation of departure statistics are available and thus, the data from these stations are analysed here.

3.2 The radio occultation technique

The signals transmitted by GNSS satellites at about 20,000 km altitude are received by Low Earth Orbit (LEO) satellites. The measurement are made during the radio occultation event, e.g. when the GNSS satellite rises or sets behind the horizon. In this case the signal is going through the limb of the atmosphere, where it is delayed and bent before it is received by the LEO satellite. The measured phase shift of the received signal, allows the retrieval of bending angle, refractivity, and thence atmospheric variables, mainly Tdry, dry pressure and, given further *a priori* knowledge about the atmospheric state, the water vapour. A description of the RO technique can be found in Kursinski et al. [23, 22]. Since the basic measurement is based on precise timing available from atomic clocks, it offers the possibility to be traceable to the international SI standard of time (Leroy et al. [25]). This ensures the long-term stability of RO data, enables the measurements from different satellites to be analysed together if they are processed by the same centre, and thus makes them valuable for climate studies.

Station Name	Station ID	Lon	Lat	Alt [m]	Sample size
Barrow (BAR)	70027	71.32°	-156.62°	8	**931**
Beltsville (BEL)		39.05°	-76.88°	53	4
Boulder (BOU)	72471	39.95°	-105.20°	1743	60
Cabauw/De Bilt (CAB)	06260	52.10 °	5.18°	1	**494 (494)**
Lauder (LAU)	93817	-45.05°	169.68°	370	78
Lindenberg (LIN)	10393	52.21°	14.12°	98	**2726**
Manus (MAN)		-2.06°	147.43°	6	40
Ny Ålesund (NYA)	01004	78.92°	11.92°	5	**747 (745)**
Payerne (PAY)	06610	46.81°	6.95°	491	48
Potenza (POT)		40.60°	15.72°	720	49
La Reunion (REU)		55.38°	-21.08°	2200	19
Southern Great Plains (SGP)	74646	36.61°	-97.49°	320	**1862**
Sodankylä (SOD)	02836	67.37°	26.63°	179	**837**
Tateno (TAT)	47646	36.06°	140.13°	31	110

Table 3.1: *GRUAN upper-air sites that have a RS92 GRUAN data product version 2 available. The official WMO station ID is given where available, even if the station ID is currently still missing in the WMO OSCAR Surface system (`https://oscar.wmo.int/surface/index.html`) . The station name is written bold if the sample size (number profiles available from 2014 and 2015) is sufficient to calculate the departure statistics. The abbreviation of the station name as used within GRUAN is given in brackets. The SGP site is also known under the name Lamont. Longitude and Latitude values are taken from the GRUAN data product.*

Currently, approximately 2000 RO profiles are measured every day and provide global coverage. While the vertical resolution of 100 m - 1 km is comparably good, the horizontal scale is big, i.e. 100-300 km around the tangent point (see figure 3 in Anthes [2]). BA profiles can be retrieved from the measured phase shift of the GNSS signal, under the assumption of local spherical symmetry of the atmosphere — no additional prior information is required to obtain this retrieval. In contrast to other remote sensing techniques RO measurements are nearly independent of the weather conditions and the profiles are retrieved from the higher atmosphere down into the boundary layer, the lowest layer of the atmosphere. An overview of the characteristics of RO measurements can be found in Anthes [2].
This report uses the near real time data of the US-Taiwanese Constellation Observing System for Meteorology, Ionosphere, and Climate (COSMIC) - FORMOSAT-3 mission (here referred to simply as COSMIC) measured in 2015. More details about the retrieval of the RO Tdry departures and the quality control applied for RO BAs can be found in Tradowsky [35].

The RO technique does not provide a direct measurement of temperature, but a retrieval is used to calculate the temperature from the time delay of a signal using a priori information. The requirement of *a priori* to calculate the temperature, implies that a temperature null-space exists in the RO retrieval. This means that some atmospheric profile perturbations do not affect the measured values. For the theory about null-spaces see Rodgers [29] (section 2.2.1) and for a description of the specific RO null-space Tradowsky [35]. This null-space

is a fundamental limitation of the RO retrieval. Due to the RO temperature null-space the technique applied here to estimate RS temperature biases using RO as reference, will only be able to estimate the contribution to the RS biases that the RO observations can determine uniquely. The assimilation of RO in NWP systems (Healy [16]) and reanalysis (Poli et al. [27], Simmons et al. [30], Kobayashi et al. [21]) is seen to anchor the temperatures at around 100 hPa, which is an indication that RO is able to provide useful bias information at these levels.

3.3 Radiosonde data

More than 800 upper-air sites launch RS on weather balloons to measure vertical profiles of temperature, humidity and, depending on the RS type, pressure. Many manufacturers correct the radiation bias in the RS temperature and humidity profiles before the data are released. Even after this correction, the temperature profiles can have substantial biases that vary with the solar elevation angle (SEA), but also depend on post-flight processing applied at the ground station. The RS temperature bias is commonly calculated per sonde type (see e.g. He et al. [15], Sun et al. [34, 33]), though Milan and Haimberger [26] found a variation of the temperature bias for stations launching the same sonde type, supporting the approach to calculate the bias separately for each station, as done here. An thorough evaluation of sources of biases in RS measurements can be found in Dirksen et al. [9].

During this study 'best estimates' of RS bias corrections profiles for individual upper-air sites are calculated to be applied in a forecast impact study. The bias correction is calculated for 852 stations that submitted data to the GTS, which were subsequently assimilated into the Met Office UM during 2015. Outliers in the RS dataset are rejected based on the Median Absolute Deviation (MAD) criterion as described in Tradowsky [35]. If an insufficient number of RS were launched at a given station, the bias correction is set to a constant value of 0.1 K. This *default* value is chosen because in the Met Office NWP system, the reading of TEMP profiles results in a bias of -0.05 K that is caused by a rounding issue in the conversion from degrees Celsius to Kelvin (see Ingleby and Edwards [20]). Additionally the encoding/decoding of the RS measurement in TEMP format causes an offset, e.g. -0.095 K for the RS92 with DigiCORAIII processing (see Ingleby and Edwards [20]) which leads to a combined bias of almost -0.15 K in the RS92 data within the Met Office NWP system. Considering that the the offset from encoding/decoding might be smaller for other RS types a value of 0.1 K is chosen for the preparation of the forecast impact study.

Two small changes in the preparation of the RS data set are implemented in comparison to Tradowsky [35], i.e. if no RS temperature is available on one of the standard pressure levels, the temperatures at the adjacent levels are interpolated to the missing level. Also, in cases where multiple temperatures are given on a single pressure level, and these do not agree, the mean value of them is used as long as the difference between them is smaller than 0.20002 K. This threshold was chosen after checking which differences occur. It is not clear why TEMP profiles with different temperatures at one level appear.

3.4 Model

The Met Office global NWP system serves as a transfer medium by providing the model background for the RO and RS profiles. This reduces differences that are caused by im-

perfect co-locations. The model version used here is described in Walters et al. [37]. The resolution of the model is N768L70, which corresponds to a grid length of about 17 km in the mid-latitudes. The time step of the model is 7.5 minutes, though the background values are linearly interpolated in time from 3-hourly fields (this is not a large source of error).

4 Preparation of the forecast impact study

One objective of this project is to prepare RS temperature bias correction profiles to be used in a forecast impact study. The bias corrections are based on the correction calculated using the technique described in Tradowsky [35], but, as these corrections only cover the stratosphere, the bias correction profiles are extended to the surface as described in section 4.1. Furthermore, for some stations a bias correction based on Tradowsky [35] is only available for certain SEA ranges. To estimate a correction for all SEA ranges, a combination of different SEA ranges is implemented here to avoid cases where no correction would be applied otherwise. This and other details for the implementation of stratospheric bias corrections are given in section 4.2.1.

This chapter describes the details used to provide a best estimate of the bias correction to be applied in a forecast impact study. This best estimate needs to be calculated with one algorithm for all stations worldwide, as this method is meant to be used operationally if the forecast impact study gives positive results. Therefore it won't offer the best possible solution for every individual station, but the aim is to find a good solution for most upper-air sites. The resulting bias correction profiles are provided for 852 stations and four SEA ranges, i.e. high, low, dusk, night in a text file ('station list') which is ready to be used in a forecast impact study.

4.1 Tropospheric bias correction

The method described in Tradowsky [35] is used here to calculate the bias corrections in the stratosphere, down to an altitude where the humidity becomes significant and the Tdry retrieval can no longer be used. To apply the bias correction in a forecast impact study, the bias correction profile needs to be extended into the troposphere.

Two possibilities of how to extend the bias correction profile to the ground are discussed here and the option (2) is implemented to be applied in a forecast impact study.

1. Using Vaisala RS92/RS41 departure statistics from night-time laucnhes as an unbiased reference to estimate the tropospheric RS bias for other RS types.
2. Use a default value of the bias correction in the troposphere with a smooth transition to the stratospheric bias correction.

4.1.1 Using Vaisala RS92/RS41 night-time statistics to estimate the tropospheric temperature bias

While this study uses a constant bias correction of 0.1 K in the troposphere with a smooth transition to the stratospheric bias corrections, the option of using RS92 background departures to calculate a tropospheric bias correction will be evaluated here. For this approach, the assumption is that the RS92 temperature profile below 150hPa is unbiased. Thus, the departure of the RS92/RS41 from the model background estimates the model bias. For stations launching different RS types, the low altitude bias correction could then be calculated from the model bias and from the O-B statistics calculated for the respective station. As the model bias might depend on the latitude, it is conceivable to calculate the model bias separately for different latitude bands. If a sufficient sample size of GRUAN profiles would be available in all latitudes, they could provide a high-quality reference to calculate the model bias. Though, as a Vaisala RS92 GRUAN data product does exist for 14 GRUAN sites only (see table 3.1)

this is not feasible.

Worldwide our RS dataset includes 191 stations that use RS92s or RS41s for at least 90% of their launches. This includes RS92 sondes of the types 14 (8 sites), 79 (19 sites), 80 (108 sites), 81 (44 sites) and RS41 sonde with the type 41 (11 sites) and one station launching a mix of the Vaisala RS types. Figure 4.1 shows all those upper-air sites that launch at least 95% Vaisala RS92 or RS41. Many stations launching Vaisala RS92 or RS41 are based in Europe, Australia and South America, though also some tropical and high latitude stations exists, e.g. 9 stations on the Antarctic continent. Thus, using all Vaisala RS92 and RS41 stations, it might be feasible to calculate the model background bias for 30° latitude bands, i.e. from 90°N-60°N, from 60°N-30°N, from 30°N 0° , from 0°-30°S, from 30°S-60°S and from 60°S-90°S.

The mean background departures for individual Vaisala stations are shown in Fig.4.2, where the colours present different 30° latitude bands. The departures stay below 0.5 K below 150 hPa for most stations. Between 100-50 hPa negative departures occur for low latitudes, i.e. mainly between 30°N and 30°S. These negative departures are due to a known warm bias around 100 hPa in the Met Office NWP system (see Hardiman et al. [13]).

The approach described here is similar to the RS bias correction applied at ECMWF, which is based on the assumption that RS92 night-time launches of one RS92 type are bias free. At ECMWF, the difference between the RS92 night-time temperature and the ECMWF model first guess is used to estimate the model bias, which is assumed to be identical over the whole globe (see Agustí-Panareda et al. [1]). In contrast to ECMWF, which is using the RS92 night-time launches to correct the whole RS temperature profile of other RS types, in this project the stratospheric bias corrections are calculated using RO BAs as an unbiased reference. The BA departures are calculated and are propagated into Tdry space to estimate the RS temperature bias. Therefore only a tropospheric bias correction is discussed here. Figure 4.3 shows the departures statistics for all stations launching 90% Vaisala RS92/RS41 sondes for the pressure levels between 1000-100 hPa. At most levels the departure statistics stay below 0.5 K, with larger departures only near the ground and at the 100 hPa level. At the 100 hPa level the larger departures are calculated at the tropical RS stations revealing the model bias discussed above.

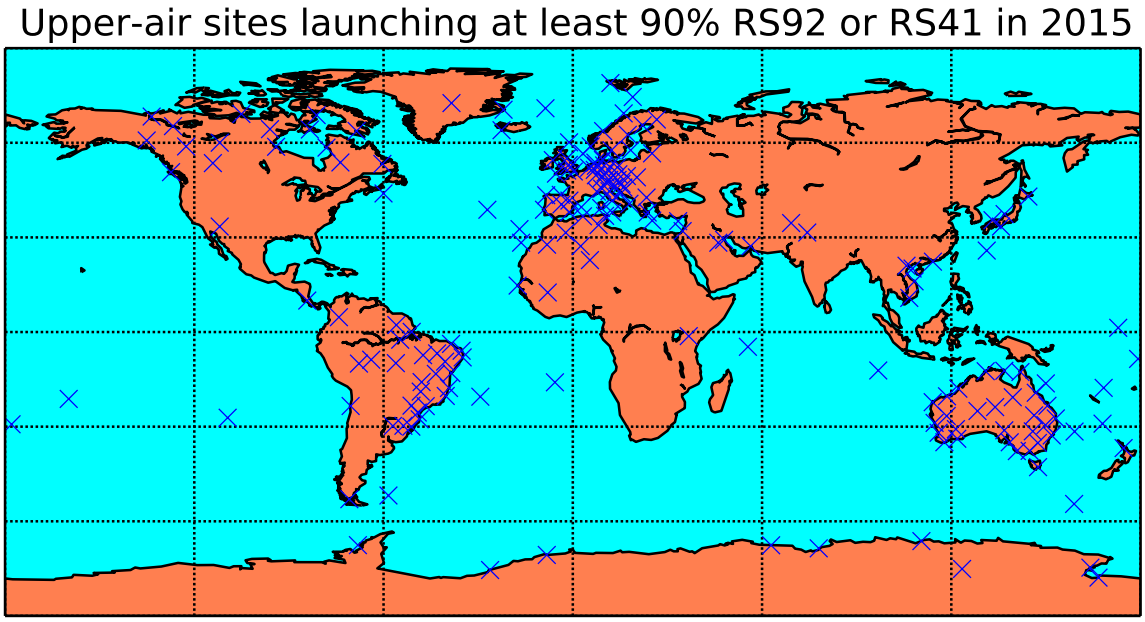

Figure 4.1: *Upper-air sites that launch 90% of the same Vaisala RS92 or RS1 type.*

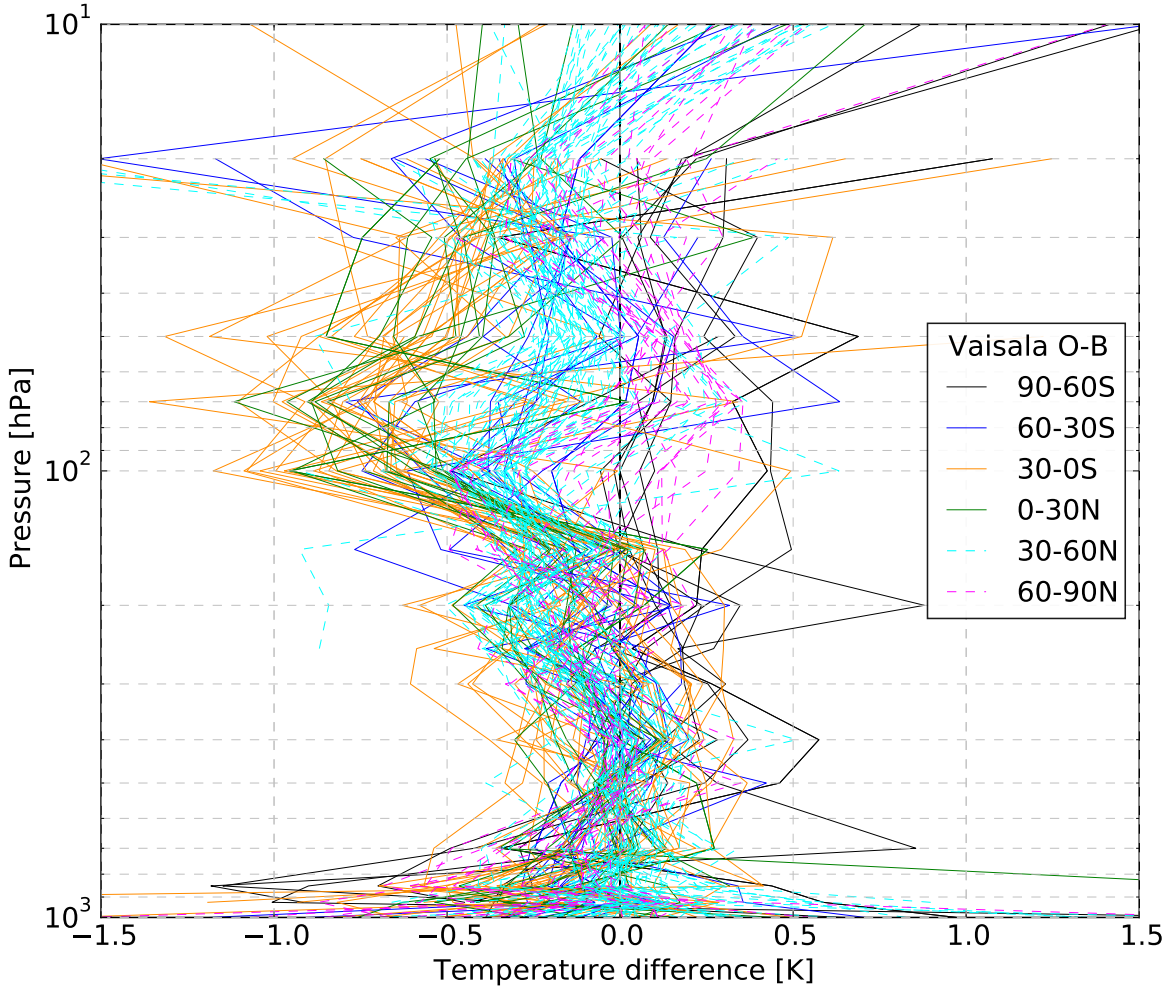

Figure 4.2: *Mean night-time O-B profiles for all sites launching at least 90% Vaisala RS92 or RS41.*

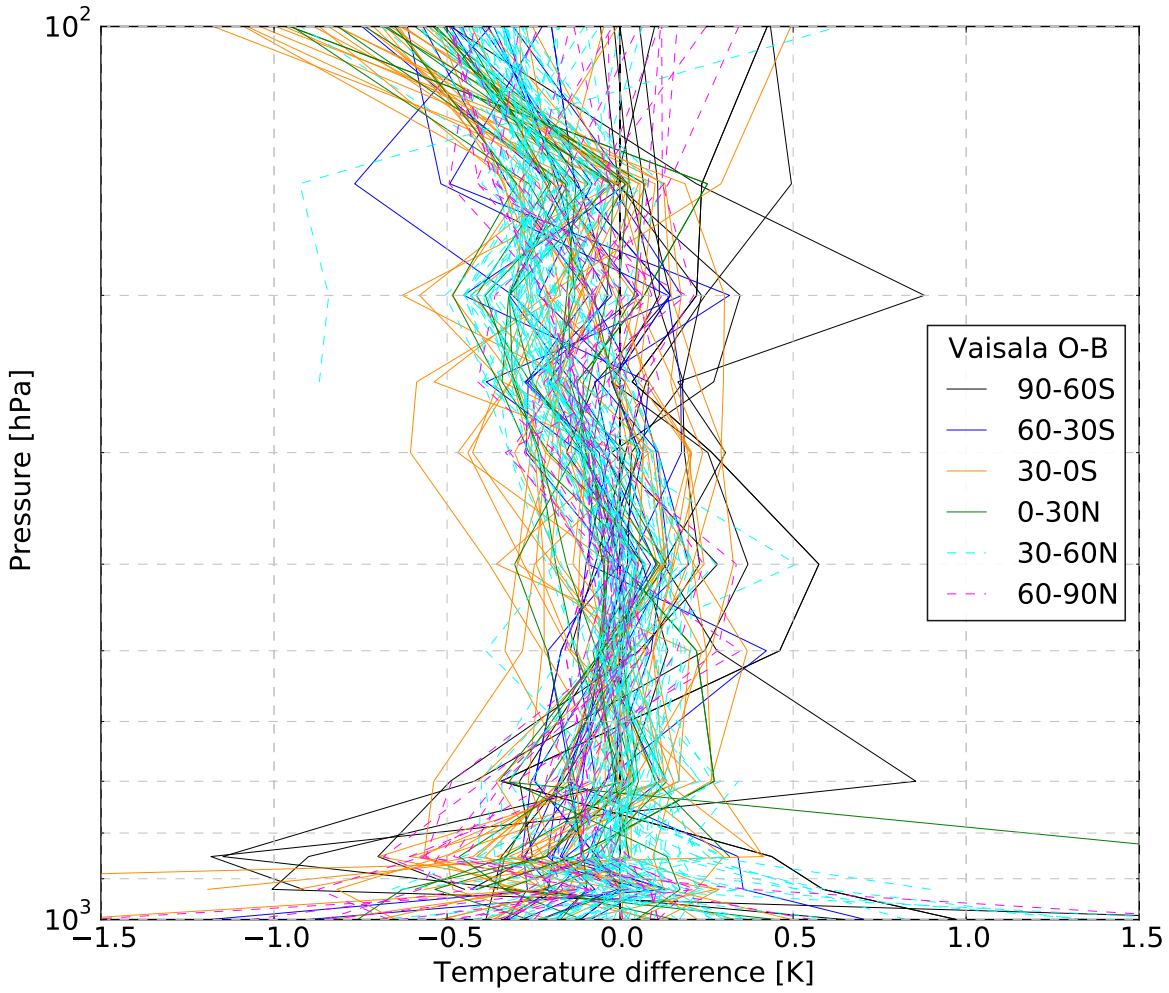

Figure 4.3: *Mean night-time O-B profiles for all sites launching at least 90% Vaisala RS92 or RS41. Altitudes below the pressure level of 100hPa only.*

4.1.2 Smooth transition of the stratospheric bias correction towards a default value in the troposphere

As tropospheric RS temperature biases are rather small (Bruce Ingleby, personal communication), it is conceivable to leave them uncorrected prior to the assimilation into the Met Office global NWP system. A smoothing of the bias correction below the lowest altitude where a correction is calculated using the method from Tradowsky [35] is required to avoid an abrupt change in the assimilated RS temperature profile. The bias corrections are smoothed to the default value of 0.1 K, rather than 0 K, as there is a known offset from TEMP decoding and from rounding in the Met Office system (see section 3.3).

To find a suitable smoothing algorithm, using a part of a cosine function as well as a linear decrease to 0.1 K is tested. Using a cosine function, the distance over which the smoothing takes place is constant which leads to a different number of standard pressure levels that are affected by the smoothing. Applying a linear decrease to 0.1 K, the same number of pressure levels are affected for each station, but the impacted distance varies. The figures 4.4 to 4.7 show different smoothing algorithms for 14 randomly chosen stations. The linear decrease

over 2 levels is shown in pink and all other lines present a smoothing using parts of a cosine function. The wave numbers for the cosine are calculated as $k = \pi / transition\ thickness$, where the transition thickness is the length in kilometres after which the bias correction is smoothed to 0.1 K (this is the number given in the legend).

The smoothing is performed to achieve a flat transition to 0.1 K. While the transition should not be abrupt, it is also important to minimize the number of levels that are influenced by the lowest altitude valid bias correction. This is important as the bias in the troposphere might have the opposite sign and thus a slow transition could deteriorate the RS temperature. The analysis of the figures 4.4 - 4.7 shows that a transition length of 2-3 km leads to an abrupt change over 1-2 standard pressure levels. On the other hand the cosine smoothing with 6km transition length influences the bias correction profile over many levels, which is also not desirable. A cosine smoothing with 4-5 km transition length show a fast, but uniform smoothing to 0.1 K and thus these values are possible choices. For most stations a valid bias correction is calculated down to the altitude of the 150 hPa level, but at some, mainly tropical stations, a valid bias correction is only available at altitudes above the 100 hPa level. Thus both of these cases are taken into account. The figures 4.4 - 4.5 show the smoothing algorithms evaluated for stations that have a valid correction at pressures below 150 hPa while figures 4.6 - 4.7 are produced for stations where the standard pressure level of 100 hPa is the highest evaluated pressure. The cosine smoothing with a 4 km transition length leads to a fast but smooth transition, especially when analysing smoothing below altitudes of the 150 hPa level, but also gives appropriate results for other cases. The cosine smoothing using a transition length of 5 km gives good results for the cases where the bias correction ends at 100 hPa, but otherwise the RS temperature profile would be affected by the bias correction over a possibly to wide pressure range, i.e. from 150 hPa to 300 hPa. Based on the results of this analysis, cosine smoothing with a transition length of 4 km will be applied to all bias corrections. The linear smoothing is in some cases similar to the cosine smoothing with 4 km transition length and could thus be a suitable choice too.

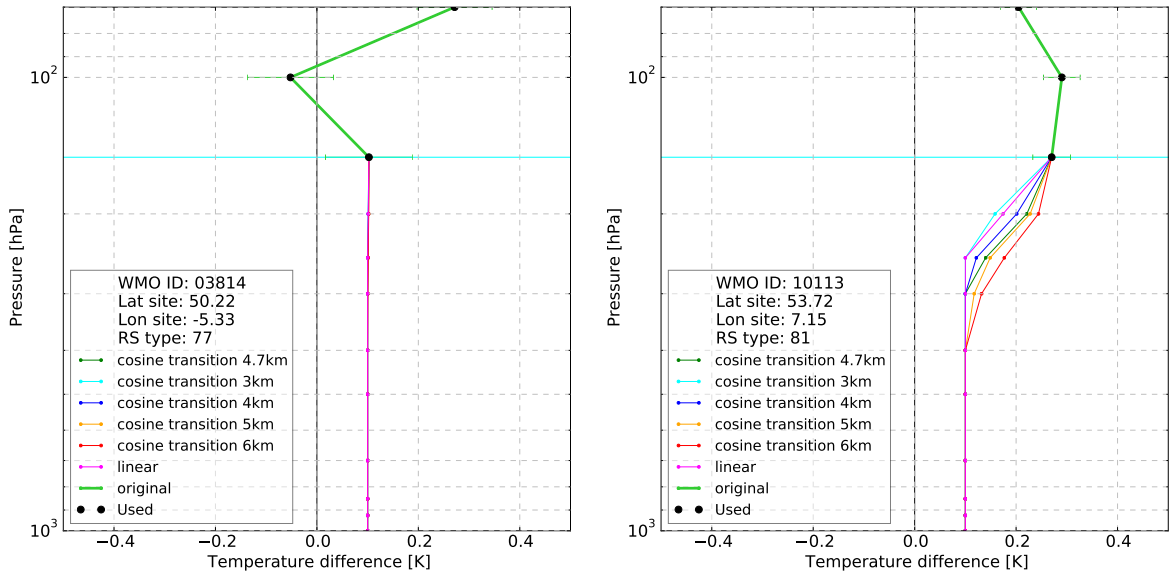

(a) WMO station ID 03814

(b) WMO station ID 10113

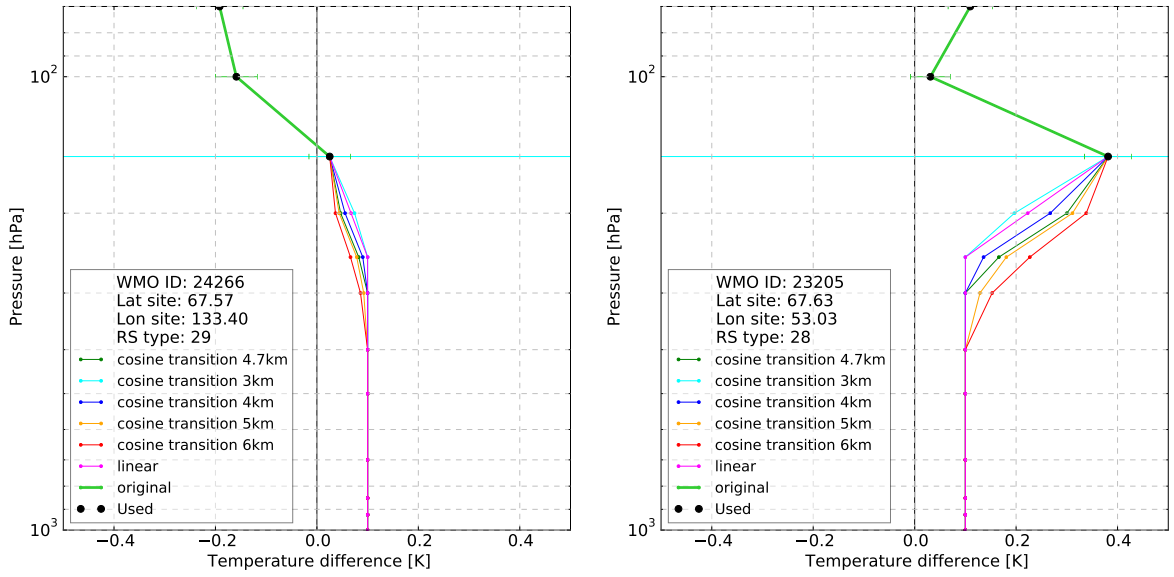

(c) WMO station ID 24266

(d) WMO station ID 23205

Figure 4.4: *Different smoothing algorithms applied at four randomly chosen upper air sites. The official WMO station IDs of the sites are (a) 03814, (b) 10113, (c) 24266, (d) 23205.*

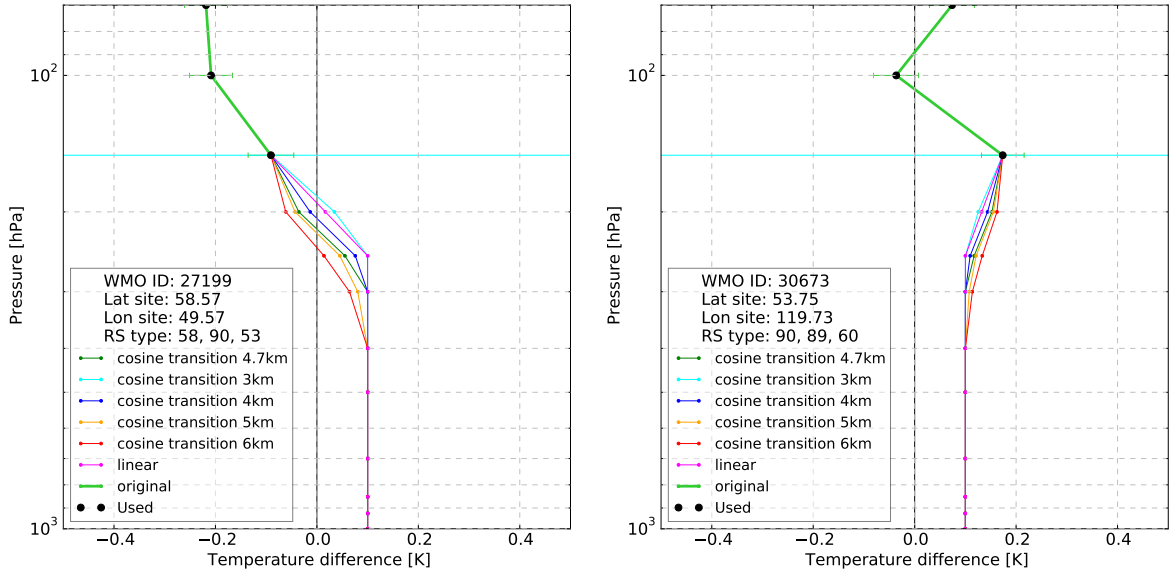

(a) WMO station ID 27199

(b) WMO station ID 30673

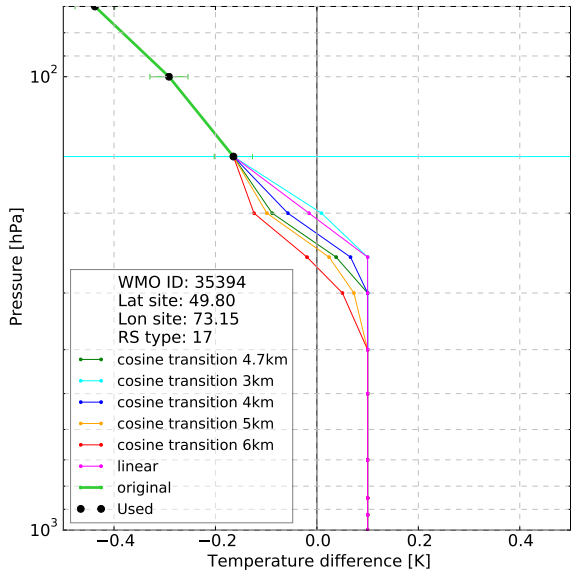

(c) WMO station ID 35394

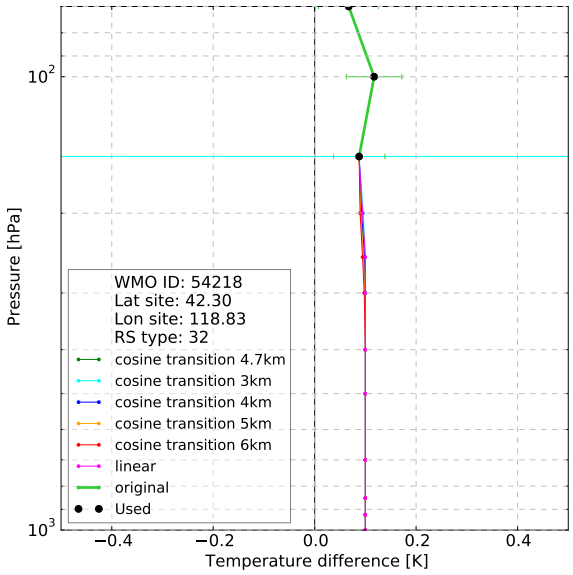

(d) WMO station ID 54218

Figure 4.5: *Different smoothing algorithms applied at four randomly chosen upper air sites. The official WMO station IDs of the sites are (a) 27199, (b) 30673, (c) 35394, (d) 54218.*

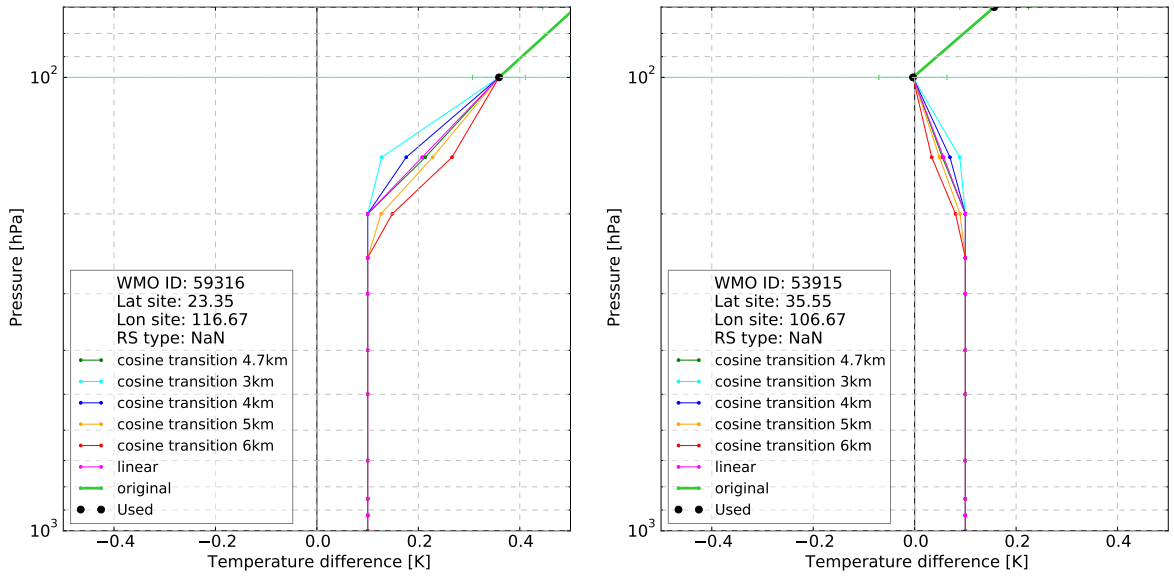

(a) WMO station ID 59316

(b) WMO station ID 53915

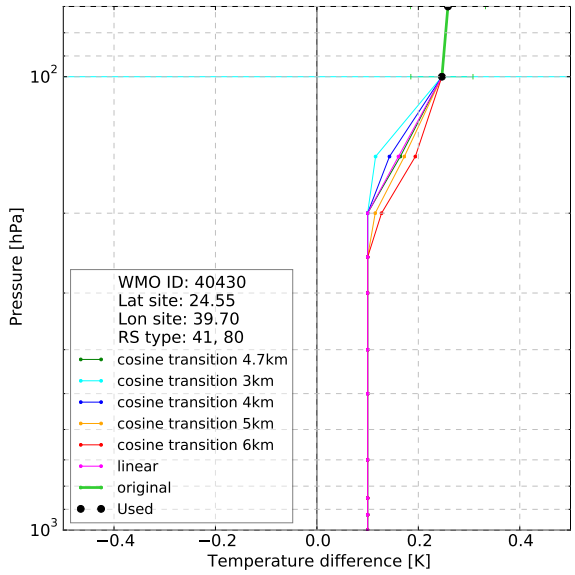

(c) WMO station ID 40430

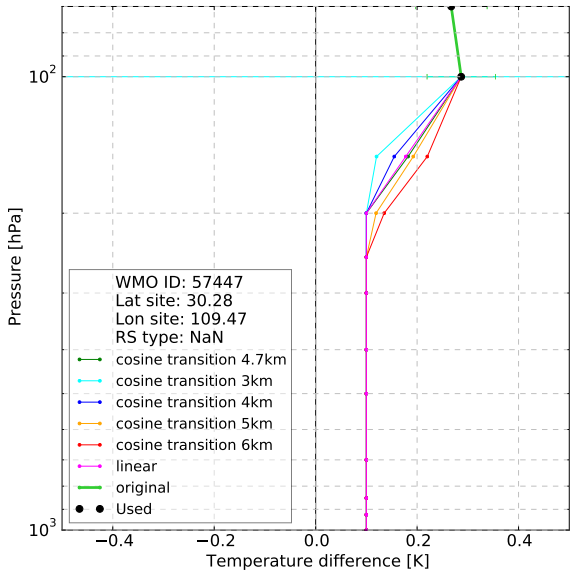

(d) WMO station ID 57447

Figure 4.6: *Different smoothing algorithms applied at four randomly chosen upper air sites. The official WMO station IDs of the sites are (a) 59316, (b) 53915, (c) 40430, (d) 57447.*

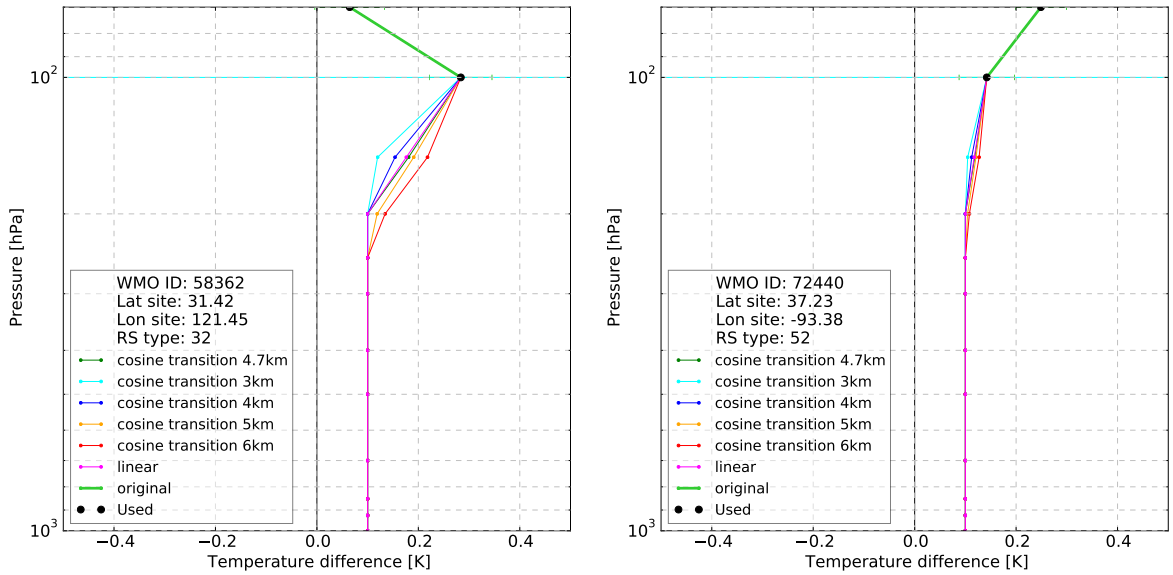

(a) WMO station ID 58362

(b) WMO station ID 72440

Figure 4.7: *Different smoothing algorithms applied at two randomly chosen upper air sites. The official WMO station IDs of the sites are (a) 58362, (b) 72440.*

As described in section 4.3, the bias correction is extended upwards above the highest altitude where a sufficient sample size is available to calculate a meaningful bias correction, i.e. the last valid value is used to correct the biases at all altitudes above this level.

4.2 Changes in stratospheric bias corrections

The ROM SAF report 26 (Tradowsky [35]) describes the method to calculate RS temperature biases using RO BAs, propagated into Tdry space as an unbiased reference. This method is applied here, to calculate the biases for all upper-air stations whose RS profiles were assimilated into the Met Office NWP system. The biases are calculated separately for four SEA ranges, i.e. 'high', 'low', 'dusk' and 'night' (see table 4.1). Though, to use the bias corrections in a forecast impact study, a combination of SEA ranges is needed if an insufficient number of RS profiles is available in a given SEA range at a given station. This is described in section 4.2.1. Furthermore, special attention is given to bias correction with large standard error in section 4.3.1. At the end of this chapter all decisions that have been made to calculate a best estimate of the bias correction based on the method described in Tradowsky [35] are summarized in table 4.2.

4.2.1 Combination of different solar elevation angle ranges

At some upper-air sites too few measurements are made within a specific SEA range (defined in table 4.1) making it impossible to calculate a meaningful bias correction for this SEA range. Though, as the bias correction calculated for high and low SEA, as well as for dusk and night tend to show similar characteristics for many upper-air stations, a combination of high/low and dusk/night can be used in these cases. Therefore, if less than 100 RS profiles are available within one SEA range at all altitudes above the 150 hPa level, the observations made within two SEA ranges (i.e. high/low and dusk/night) are used to calculate the mean

departure profile. The RO departures are also calculated using all profiles measured within the combined SEA ranges. If sufficient numbers of observations are still not available within the combined SEA ranges, the mean departures calculated from all profiles (independent of the SEA range) are used. While the combination of SEA ranges might cause problems at individual RS stations, we expect it to be better than not correcting the bias for the given SEA at a given RS station on average.

If no RS observations are available within one SEA range, the combination of two SEA ranges is used and if no measurements are available within these combined SEAs, the statistics for the other combined SEA ranges are used. Using the opposite SEA range might give inappropriate bias correction in some cases, but for some stations with large biases (i.e. many Russian ones) the bias correction profile has a similar shape for different SEA ranges. Furthermore it is unlikely that this correction will ever be applied, as they would only get used if the station would change its RS launch schedule.

For stations where even the combination of all SEA ranges does not lead to a sample size >=50 at altitudes above the 150hPa level, the default bias correction of 0.1 K is applied throughout the whole RS profile. As this affects few RS launches, it is not expected to cause major issues. It would also be possible to use a radiosonde type specific bias correction, if not enough profiles are available at one station. However, this would lead to problems if various sonde types are launched or if the radiosonde type is unknown. For stations at which between 50 and 100 profiles are available, the calculated bias correction is used, but the threshold for the standard error is decreased to 0.05 K, i.e. if the standard error of the bias correction is greater than 0.05 K, the bias correction minus the standard error is applied as described in section 4.3.1.

4.3 Extension of bias corrections above the highest valid level

The number of observations usually decreases at the top of the profile and with the smaller sample size, the standard error increases. If the sample size becomes too small, the calculated bias correction might be determined by outliers. Therefore, if less than 20 valid RS observations are available at a standard pressure level, the bias correction at this level is not used. Instead the highest valid bias correction is extended to 5 hPa.

Figure 4.8 shows the RO (blue) and RS (pink) departure profile and the bias correction profile (thick green) to be added to the RS temperature profile in a forecast impact study for the station *04360* in Greenland. The cyan coloured horizontal line gives the pressure level of the lowest altitude where a valid bias correction is calculated using RO BA as reference. The black dots mark those corrections calculated using the technique described in Tradowsky [35] that get used, i.e. for night-time launches, the highest level original correction (thin green) is not applied as the sample size is lower than 20. In figure 4.8(b) high and low SEA ranges are combined as the sample size for the low SEA range is not sufficient to calculate a valid bias correction. The grey dashed line gives the bias correction as it is calculated using only one SEA range, i.e. only RS launched in the low SEA range in 4.8(b). If no combination of SEA ranges is performed, or if no profiles are available in the original SEA range, the grey line is not visible at is is plotted below the thin green line.

Name	SEA range [degree]
High	SEA >= 22.5°
Low	7.5° <= SEA < 22.5°
Dusk	−7.5° <= SEA < 7.5°
Night	SEA < −7.5°
High/Low	SEA >= 7.5°
Dusk/Night	SEA < 7.5°

Table 4.1: *Solar elevation angle ranges and combined solar elevation angle ranges which can be used if the number of available profiles is too low.*

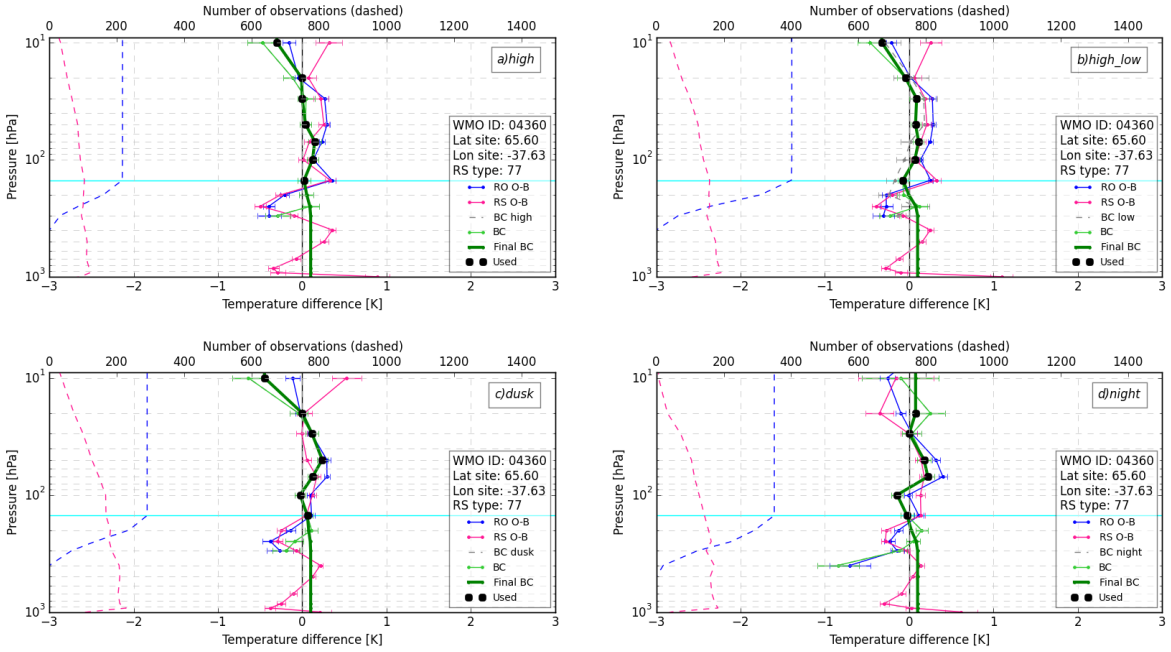

Figure 4.8: *RO Tdry departure (blue), RS temperature departures (pink) and bias correction (RO O-B minus RS O-B, green) the example site 04360 in Greenland for different SEA ranges a)-d) (see upper right corner of the subplots). The horizontal cyan line indicates the highest standard pressure level (lowest altitude) where at least 95% of the RO profiles are included. The error bars represent the standard errors (sampling uncertainty), taking into account the sample size and the standard deviation of the departures.*

4.3.1 Bias corrections with large sampling errors

Each bias correction has an associated standard error which takes into account the sample size of RO and RS and the standard deviations within the sample. If this standard error is greater than 0.1, a 'minimal' bias correction is applied. For this minimal bias correction, the standard error is subtracted for positive bias corrections and added for negative bias corrections, which means that the final bias correction is going through the inner error bar. If this would lead to a change in the sign of the bias correction, it is set to 0 K.

Figure 4.9 presents the statistics for a Russian upper-air site, where a minimal bias correction

is applied for all but the night-time launches.

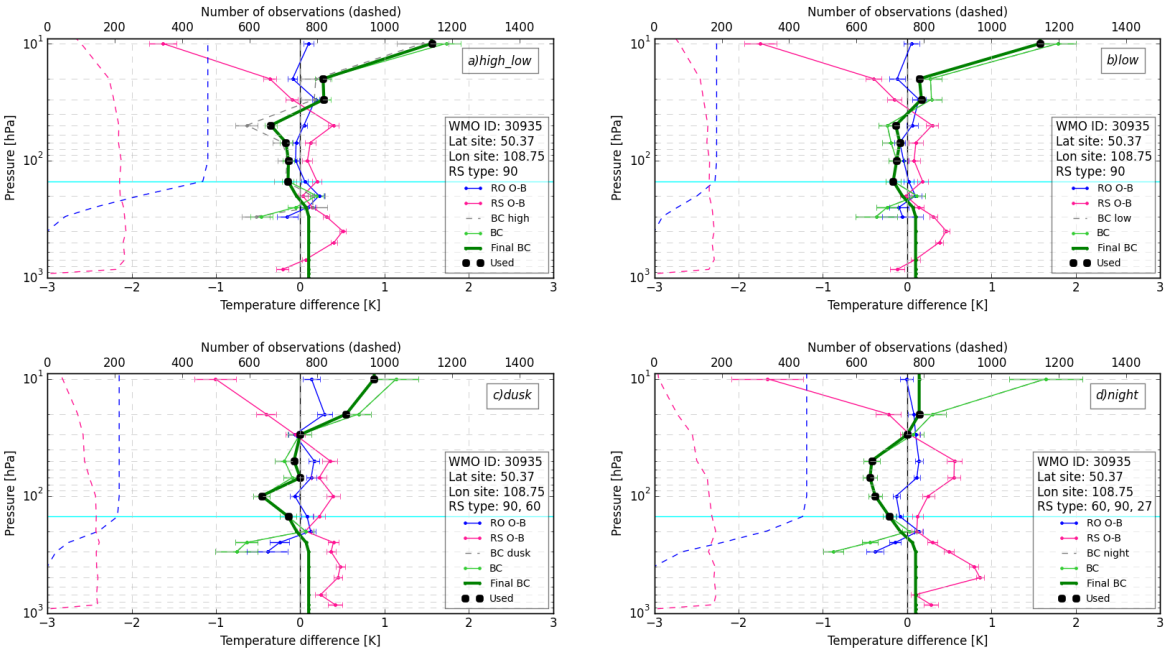

Figure 4.9: *RO Tdry departure (blue), RS temperature departures (pink) and bias correction (RO O-B minus RS O-B, green) the example site 30935 in Russia for different SEA ranges (a)-(d). The horizontal cyan line indicates the highest standard pressure level (lowest altitude) where at least 95% of the RO profiles are included. The error bars represent the standard errors (sampling uncertainty), taking into account the sample size and the standard deviation of the departures.*

4.4 Summary of the decisions made to calculate the bias corrections

To calculate a best estimate of the bias correction for all SEA ranges and all standard pressure levels, an algorithm is developed within this project. The bias RS temperature bias corrections are first calculated using RO BAs as unbiased references as described in Tradowsky [35]. These stratospheric bias profiles are then used as basis for the bias correction profiles that are prepared for a forecast impact study. The choices in table 4.2 are made within the algorithm to calculate a best estimate of the bias correction profile.

4.5 Seasonal dependence

The bias corrections calculated based on the method described in Tradowsky [35] and the method for the preparation of a forecast impact study described here, give good results for most upper-air sites. Though, the combination of SEA ranges leads to larger differences between the combined statistics (green line) and the statistics for an individual SEA range (grey dashed line) at some Russian stations. The problem occurs only for the low SEA range, e.g. at the stations 27038 (see Fig.4.10) and 22820 (see Fig.4.11), where the number of profiles in low SEA is below 100 profiles and thus the combined profiles are used. This could be an effect of the season, as the launches in the low SEA range at the given stations might only happen at a certain season of the year, while the RO profiles that are used in low

Parameter	Value
minimum number of profiles at a station	50
minimum number of profiles in SEA range	100
minimum number of profiles at any level	20
threshold for standard error	0.1 K
threshold for standard error, < 75 profiles at station	0.05 K
correction below lowest valid level	smoothing to default bias correction
applied smoothing	cosine, 4 km transition thickness
default bias correction	0.1 K
correction above highest valid level	extension of highest valid value upwards

Table 4.2: *Summary of the parameters chosen within the algorithm that calculates a best estimate of the bias correction for all SEA ranges at all stations that were assimilated into the Met Office UM during 2016.*

SEA range, are calculated from the whole year.

While currently the statistics for combined SEA ranges are used at all stations, further investigation into the seasonal dependence is needed. In section 6.3 the seasonal dependence is analysed for two GRUAN sites.

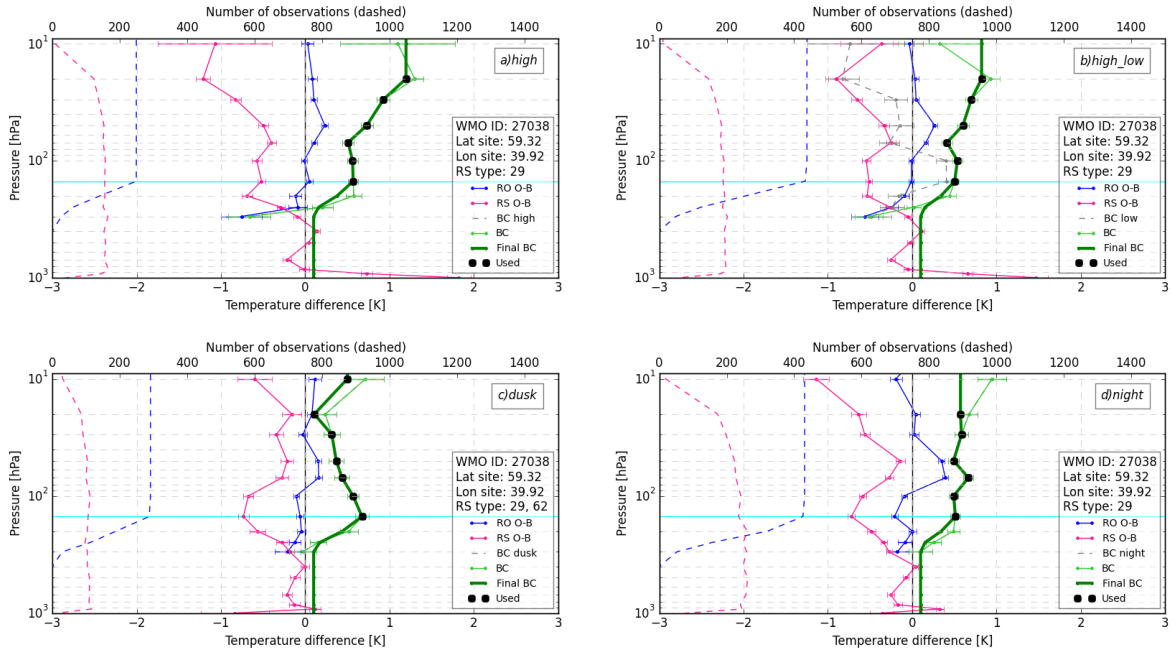

Figure 4.10: *RO Tdry departure (blue), RS temperature departures (pink) and bias correction (RO O-B minus RS O-B, green) the example site 27038 in Russia for different SEA ranges (a)-(d). The horizontal cyan line indicates the highest standard pressure level (lowest altitude) where at least 95% of the RO profiles are included. The error bars represent the standard errors (sampling uncertainty), taking into account the sample size and the standard deviation of the departures.*

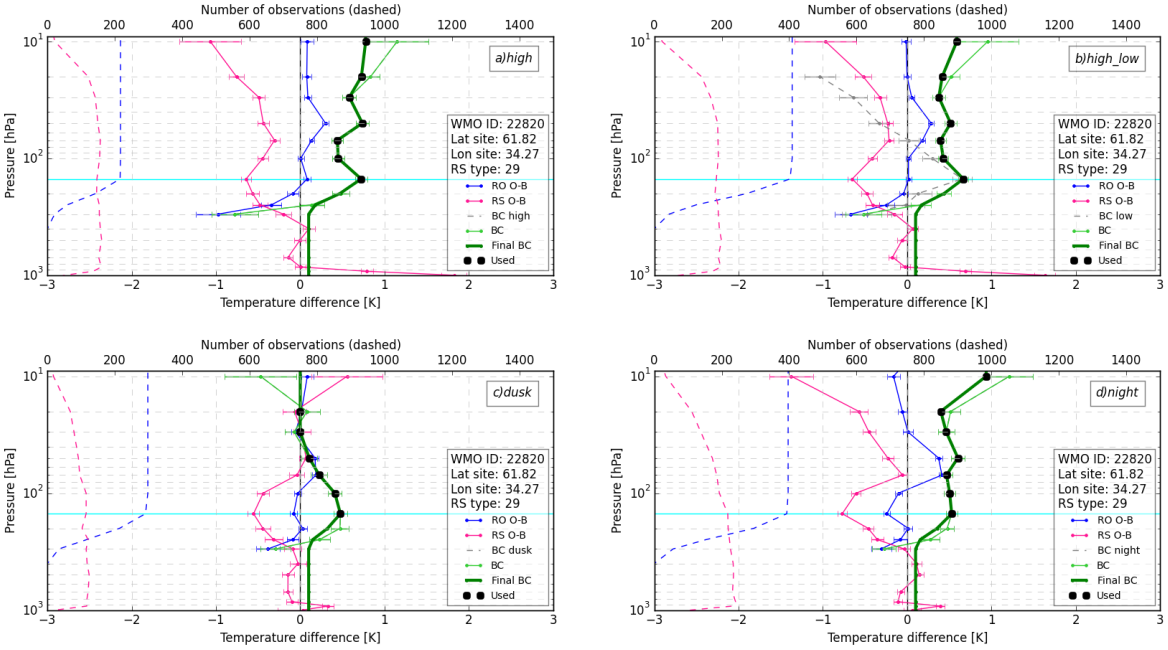

Figure 4.11: *RO Tdry departure (blue), RS temperature departures (pink) and bias correction (RO O-B minus RS O-B, green) the example site 22820 in Russia for different SEA ranges (a)-(d). The horizontal cyan line indicates the highest standard pressure level (lowest altitude) where at least 95% of the RO profiles are included. The error bars represent the standard errors (sampling uncertainty), taking into account the sample size and the standard deviation of the departures.*

5 Investigation of the structural uncertainty in the Tdry departure statistics

As described in Tradowsky [35], the technique used here for the calculation of the RO Tdry departures uses BA departures, which are set to zero above an impact height of 35 km before they are propagated into Tdry with a tangent linear retrieval. This chapter will compare the cut-off applied here to a method similar to the conventional RO retrieval which uses statistical optimization techniques to smooth the BAs above an altitude of 30-40 km (see Ho et al. [18], table 1).

Using the terminology from Rodgers [29], the Tdry retrieval used in this study is an 'exact' retrieval which is sensitive to noise, as it tries to fit noisy measurements exactly. As the noise in the RO BAs increases with altitude, statistical optimization techniques are applied in the conventional Tdry retrieval to blend the RO BA profile with a climatological BA profile. Thus, with increasing altitude, the information content from the measurement decreases, as the weight on the *a priori* profile increases. As the high level BA information influences the retrieved temperature at all levels below, the choice of *a priori* climatology impacts the whole retrieval. As this is not desirable when estimating biases of RS, which only reach about 30-35 km, we set the BA departures above a certain impact height to zero. Thus, the downward propagation of *a priori* and model information is limited, which would otherwise lead to inconsistent departure statistics for the two observation types. Importantly, using BA departures up to higher levels would invalidate the central assumption for a double differencing approach, i.e. that the model biases are constant over the separation distance. Using the model information in the RO retrieval up to e.g. 55 km, would mean that the model biases are included up to 55 km, while they are only used up to $\approx$ 35 km in the calculation of the RS departures.

Using an upper cut-off does not require an *a priori* BA profile, but can be understood as an extreme case of statistical optimization. It is equivalent to using 0% climatology below 35 km impact height and 100% climatology above 35 km for both the RO and the background BA. In this case the departures will be zero above 35 km impact height and be independent of the climatology below 35 km.

In Fig.5.1 the TL Tdry departures for different cut-off impact heights (including no cut-off) are compared with Tdry departures calculated applying high level BA optimization. In addition, Fig. 5.1 shows the non-linear Tdry departures for the example site in western Russia. Note that the similarity of the green line (no cut-off) and dashed black line (non-linear) indicates the accuracy of the linearisation. Major impact on the Tdry departures results from setting solely the highest RO BA departure value to zero prior to the TL Tdry calculation (compare green and gray line). Setting the highest value to zero minimizes the strong influence of the highest level BA departures and thus is having a strong effect. Similar figures are shown in Tradowsky [35] for five example sites and the reasons for the major influence of the highest level BA departure is discussed in detail in Tradowsky [35] and Burrows and Healy [6].

The dot-dashed curves in Fig.5.1 show Tdry departures calculated using RO BAs that are blended with the background values, in an analogous way to how BAs are blended with climatology in conventional refractivity retreivals that use statistical optimisation. Here, the

background information has 50% weight at 47 km (red) and 32 km (violet), respectively. Here, the aim is to illustrate which effect different implementations of statistical optimization can have on the retrieval. The "statistically optimised" RO BAs are calculated as: $\alpha_{RO_{smooth}} = w \cdot \alpha_{RO} + (1-w) \cdot \alpha_{climatology}$, where the weight w is calculated as $w = \frac{\sigma^2_{climatology}}{\sigma^2_{climatology}+\sigma^2_{RO}}$ and $\alpha_{climatology}$ is, in fact, the background BA. The assumed observation/model error is set to $\sigma_{RO} = 2$ microradians and the error in the climatology is assumed to be 1% (i.e. $\sigma_{climatology} = 0.01 \cdot \alpha_{climatology}$, violet dot-dashed line) and 10% (i.e. $\sigma_{climatology} = 0.1 \cdot \alpha_{climatology}$, red dot-dashed line), respectively. When using 50% *a priori* at 32 km, the Tdry departures closely follow the line for 35 km cut-off (blue), with the biggest difference of about 0.1 K at the top level. Similarly using 50% *a priori* at 47 km closely resembles a cut-off at 50 km. Thus, setting the departures above a certain altitude to zero gives similar results than blending the RO and model BA profile with climatology, but it allows better control of the flow of information.

As an example of the amount of information the observation provides in a conventional statistical optimisation retrieval, using a typical value of a climatological BA at 55 km impact height ($\approx$ 10 microradians) and an assumed 10% error on the climatology, the weight given to the observation at 55 km would be 0.2, which means that, at 55 km, the RO observation provides 20% of the information and the climatology 80%.

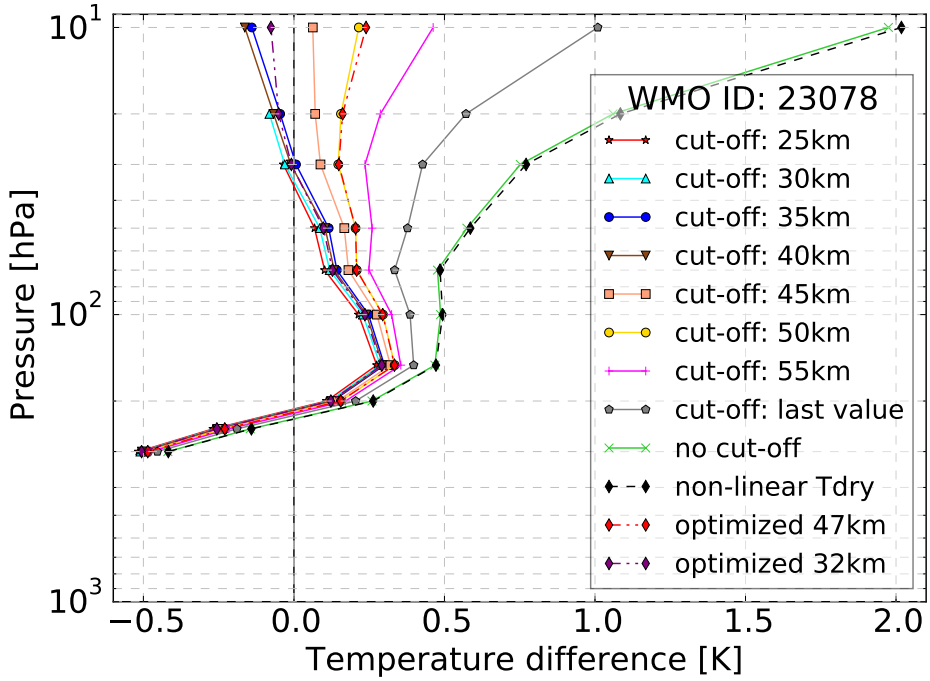

Figure 5.1: *Sensitivity of the mean Tdry departure to different upper cut-off impact heights. The mean Tdry departure is calculated from up to 842 RO profiles within a 500 km radius around the example site 23078 in western Russia. Also shown is Tdry departure calculated with the non-linear retrieval (black dashed) and the Tdry departures calculated using statistical optimization with 50% of the background BA used at 32 km (purple dash-dotted) and at 47 km (red dash-dotted), respectively.*

Like every assumption that is made in a retrieval, reasonable variations in the choice of the upper cut-off height contribute to the structural uncertainty. This is analogous to the structural uncertainty related to choosing a climatology/weighting to be used in the calculation of statistically-optimized bending angles (see difference in dash-dotted lines in Fig.5.1). Ho et al. [18] estimates the structural uncertainty resulting from different processing schemes as the differences and standard deviations between retrievals from individual processing centres and the inter-centre mean. For global RO Tdry calculated from different processing centres, Ho et al. [18] find mean differences between -0.27 K and 0.15 K in an altitude range of 8-30 km.

To give an estimate of the structural uncertainty generated by the choice of the cut-off height, the range (largest minus smallest value) of the departures calculated for cut-off heights between 35 km and 55 km is shown in Fig.5.2. Remember, this study is not using high level statistical optimization and thus the high level departures are dominated by noise. Thus the departures above 55 km are not included in the estimation of the structural uncertainty. The black line is calculated from ≈ 77,000 globally distributed COSMIC-6 BA profiles measured during 2014, while the other lines are calculated from all COSMIC BA profiles within 500 km around the respective upper-air site (the station ID is given in the legend). In general, the structural uncertainty increases with decreasing pressure. The structural uncertainty of the global statistics is calculated to estimate the typical behaviour. It stays below 0.2 K at pressure levels above 50 hPa and increases to about 0.47 K at 10hPa. Our estimation of the global structural uncertainty resulting from choosing an upper cut-off is thus similar to the structural uncertainty resulting from different RO processing schemes as presented in Ho et al. [18].

The structural uncertainty is appreciably lower at the Russian upper-air site with the station ID 25913 and appreciably larger at the Indonesian site (ID 97560). Strong vertical gradients, caused by gravity waves above this tropical site in Indonesia, could explain the strong dependence on the cut-off height, but also the comparably small sample size (<=242 ROs, compared to <= 1093 for site 25913) could affect the results.

Estimating the structural uncertainty is of major importance for climate studies. For the purpose of estimating RS biases, the range of the departures between 35 km and 55 km might though be an overestimation of the uncertainty, as a cut-off impact height of 55 km would invalidate the central assumption for the double-differencing technique, i.e. the model bias is constant over the separation distance (see Burrows and Healy [6]).

In summary, the application of the 35 km cut-off is justified for two reasons. First, this reduces the effect of noisy, and arbitrarily extrapolated RO data from the upper stratosphere and mesosphere that would otherwise affect all calculated bias corrections. Second, it avoids the influence of model biases above the RS altitude range which, if the cut-off was not applied, would result in biased RO departures that would persist in the bias corrections after the double differencing.

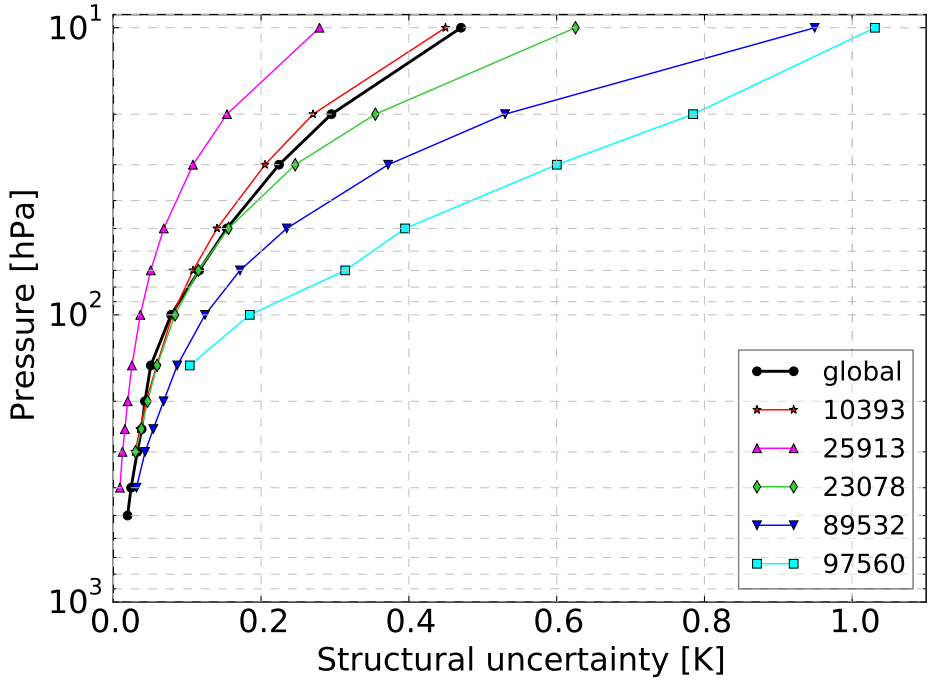

Figure 5.2: *Basic estimate of the structural uncertainty in the RO departures based on the range of the Tdry departures calculated from BA departures with different upper impact height cut-offs between 35 km and 55 km.*

For completeness the departure statistics for different upper cut-off heights are shown for all example RS sites discussed in Tradowsky [35] in Fig. 5.3 (figure taken from Tradowsky [35]. The range of the departures depends on the station investigated and is increasing with decreasing pressure as can also be seen in Fig. 5.2. For all but the Indonesian station, the departures become more positive with an increasing cut-off height. This indicates a model bias that propagates into the Tdry departures through the Tdry retrieval chain. Burrows and Healy [6] show that the tangent linear Tdry retrieval propagates high level model biases downward in the retrieval chain by comparison of Tdry departures calculated using either ECMWF or Met Office background fields. For worldwide departures calculated from ≈ 77,000 COSMIC-6 profiles (see Fig.5.4) the cut-off at 35 km leads to a departure profile that is close to a cut-off at 55 km. The departure statistics do not develop into one direction with increasing cut-off height. Thus the model bias that is indicated by the analysis of individual stations might not be constant for the whole globe/whole year and cancel out for worldwide averaged RO BA departures.

Figure 5.5 shows the standard deviation of the Tdry departures calculated using different cut-off heights. The standard deviation increase with increasing cut-off impact height. This indicates the exclusion of noise from the statistics when setting high level BA departures to zero.

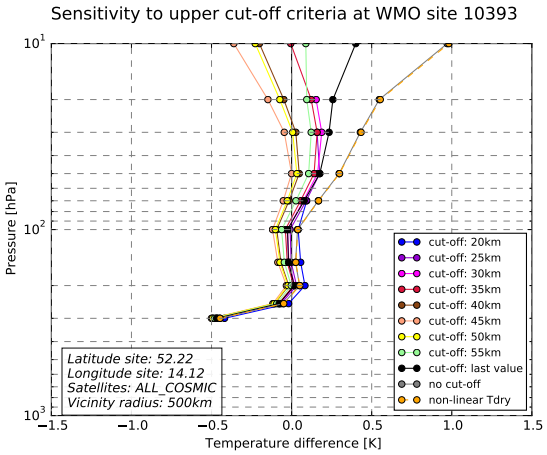

(a) Germany

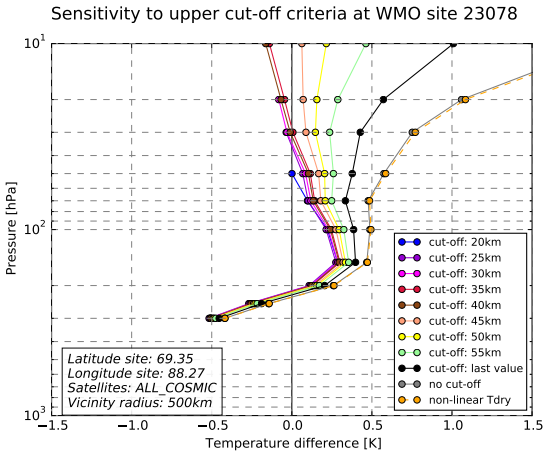

(b) Russia West

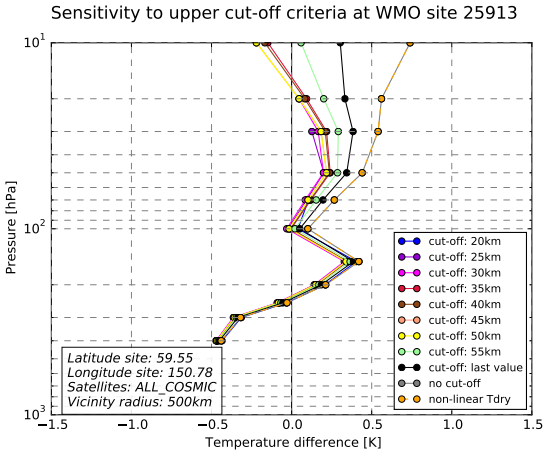

(c) Russia East

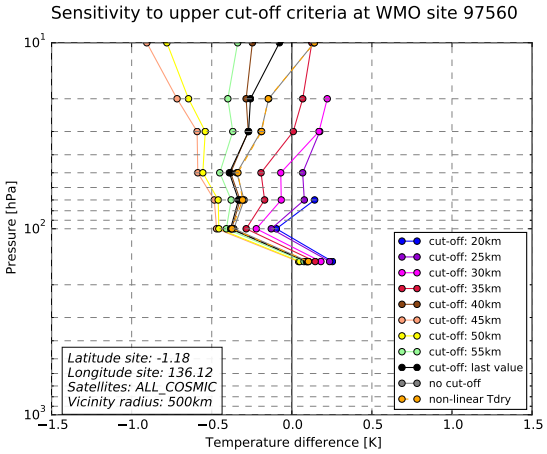

(d) Indonesia

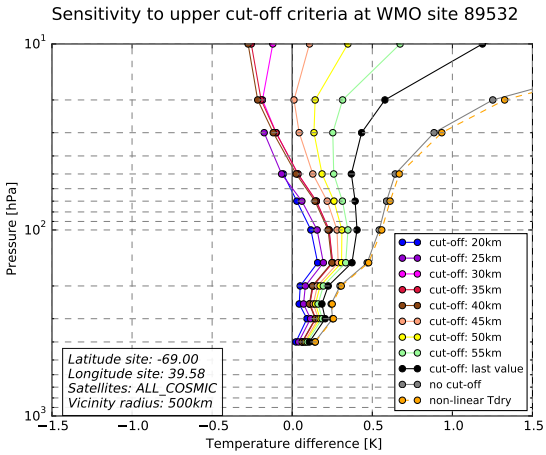

(e) Antarctica

Figure 5.3: *Sensitivity of the Tdry departures caused by different upper cut-off impact heights (all RO BA departures above the cut-off impact height are set to zero prior to the Tdry calculation).*

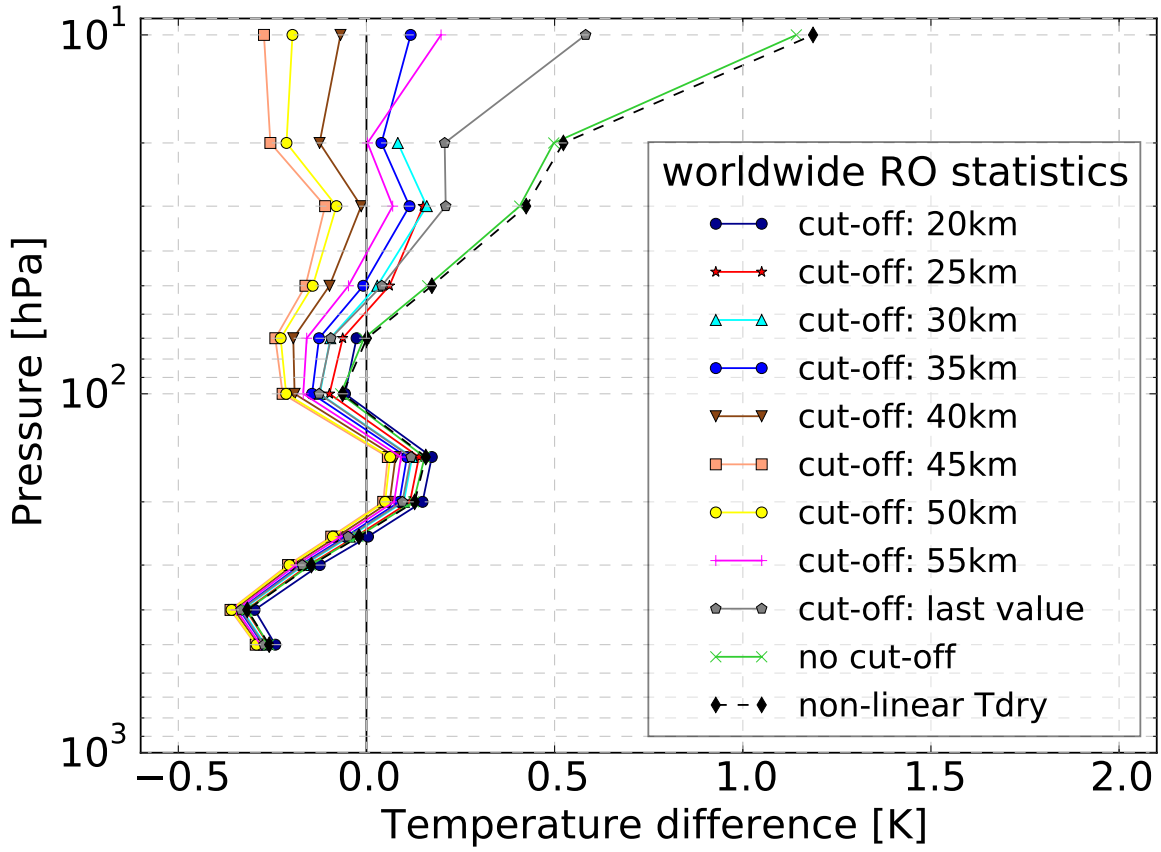

Figure 5.4: *Sensitivity of the mean Tdry departure to different upper cut-off impact heights. The mean Tdry departure is calculated from about 77,000 COSMIC-6 RO profiles worldwide. Also shown is Tdry departure calculated with the non-linear retrieval (black dashed).*

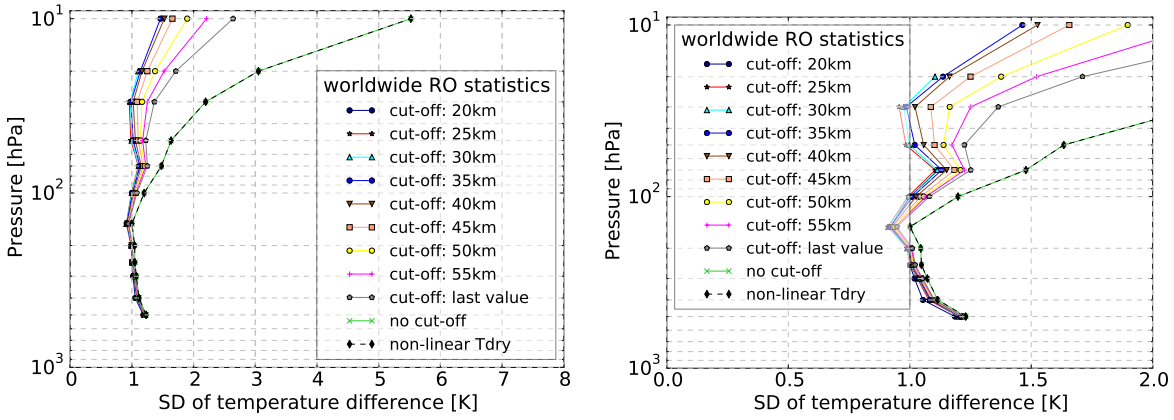

(a) ***(b)*** zoom of (a)

Figure 5.5: *Standard deviation of the Tdry departures calculated using different cut-off impact heights in the RO retrieval. In the retrieval ≈ 77.000 RO profiles measured with COSMIC-6 are used.*

6 Analysis of the GRUAN data

The double differencing technique described in Tradowsky [35] and Tradowsky et al. [36] is used here to compare GRUAN and RO observation minus background (O-B) statistics on a station-by-station basis. First, the departures of the GRUAN temperatures from the model background temperature are calculated for every GRUAN profile and then the mean departure profile at a given station is calculated on standard pressure levels.

As the GRUAN data processing does not change over years it is highly unlikely that there would be any discontinuities in the time series at any one GRUAN location resulting from data processing. The same could not be the case for vendor provided RS data which could be subject to changes in the processing. It is therefore justifiable to use the measurements made during 2014 and 2015 for this analysis. As for the analysis of RS, COSMIC BA data within 500 km of a GRUAN site are used to calculate the mean BA departure profile. This profile is then propagated into a mean Tdry departure profile using the tangent linear retrieval chain described in Tradowsky [35]. The RO Tdry departures are then compared to the GRUAN temperature departures in the dry part of the atmosphere (tropopause and stratosphere).

As both RO and GRUAN provide high quality data which are used as reference data products, good agreement between the profiles is expected. Though, while RO exhibits the highest accuracy in the upper troposphere and lower stratosphere (Kursinski et al. [22]), GRUAN has the lowest random uncertainty in the troposphere. To investigate if both data sets are consistent, it is essential to include an estimate of the uncertainty on both data sets in any comparison. The GRUAN data product includes an estimate of the uncertainty on every datum, which is propagated into the uncertainty on the mean GRUAN O-B departures. The following sections describe (i) how an uncertainty weighted average of the GRUAN departures is calculated and (ii) how the uncertainty on the mean GRUAN temperature departure is calculated from the uncertainties on the individual profiles. Furthermore, the structural uncertainty in the RO Tdry departures is estimated and finally the RO and GRUAN departures are compared and discussed.

6.1 Calculation of the mean GRUAN departures and the associated uncertainties

As the GRUAN profiles come with an estimate of the uncertainty on each datum, these uncertainties can be propagated into the uncertainties on the mean GRUAN departures from model background values. For this purpose, the variable ‘u_temp’ which is the *Standard uncertainty (k=1) of air_temperature* provided in the GRUAN data files, is used. This is the total uncertainty of temperature, which is composed of correlated and uncorrelated components (see Sommer et al. [31] and Dirksen et al. [9]). This uncertainty is propagated through the calculation of mean departures and is displayed in the uncertainty bars of GRUAN departures. The different steps in the calculation of the GRUAN departures are, (i) interpolation of temperatures to standard pressure levels, (ii) calculation of background departures, and (iii) calculation of mean background departures for every available GRUAN site.

6.1.1 Interpolation of GRUAN temperatures to standard pressure levels

The linear interpolation to the standard pressure levels is done in logarithmic pressure using the following equation

$$T_{GRUAN}(P) = (1-\beta)\cdot T_0 + \beta \cdot T_1 \tag{6.1}$$

where $\beta = \frac{ln(P)-ln(P_0)}{ln(P_1)-ln(P_0)}$, T_0 is the temperature at the next highest pressure P_0 (lower altitude), T_1 is the temperature at the next lowest pressure P_1 (higher altitude) and P is the pressure level to which the temperature is interpolated. The uncertainty on the interpolated temperature can be calculated using the error propagation equation (see e.g. Eq. 3.13 in Bevington and Robinson [4]), taking into account the uncertainty on the temperature profile, but not the uncertainty on the pressure, as:

$$\sigma_{T_{GRUAN}(P)} = \sqrt{\sigma_{T_0}^2 \cdot \left(\frac{\partial T(P)}{\partial T_0}\right)^2 + \sigma_{T_1}^2 \cdot \left(\frac{\partial T(P)}{\partial T_1}\right)^2 + 2\cdot\sigma_{T_0T_1}^2 \cdot \left(\frac{\partial T(P)}{\partial T_0}\right)\cdot\left(\frac{\partial T(P)}{\partial T_1}\right)} \tag{6.2}$$

The GRUAN RS92 version_2 data products does not include the covariance matrix which contains $\sigma_{T_0T_1}$. Therefore, the limits of the uncertainty are estimated by analysing the three limits of the correlation coefficient R, which can be used to rewrite equation 6.2 as:

$$\sigma_{T_{GRUAN}(P)} = \sqrt{\sigma_{T_0}^2 \cdot \left(\frac{\partial T(P)}{\partial T_0}\right)^2 + \sigma_{T_1}^2 \cdot \left(\frac{\partial T(P)}{\partial T_1}\right)^2 + 2\cdot\sigma_{T_0}\cdot\sigma_{T_1} \cdot \left(\frac{\partial T(P)}{\partial T_0}\right)\cdot\left(\frac{\partial T(P)}{\partial T_1}\right)\cdot R} \tag{6.3}$$

where $-1 \leq R \leq 1$ is a coefficient describing the interdependence of σ_{T_0} and σ_{T_1}.

In the following, uncertainty estimates for three values of R are discussed to inform the calculation of the uncertainty on the interpolated GRUAN temperature.

1. Uncorrelated uncertainties, $R = 0$:
   If the uncertainties are uncorrelated, the covariance term is zero and the uncertainty on the interpolated temperature can be calculated as:

$$\sigma_{T_{GRUAN}(P)} = \sqrt{\sigma_{T_0}^2 \cdot \left(\frac{\partial T(P)}{\partial T_0}\right)^2 + \sigma_{T_1}^2 \cdot \left(\frac{\partial T(P)}{\partial T_1}\right)^2} = \sqrt{\sigma_{T_0}^2 \cdot (1-\beta)^2 + \sigma_{T_1}^2 \cdot \beta^2} \tag{6.4}$$

2. Completely negatively correlated uncertainties ($R = -1$):
   If σ_{T_0} and σ_{T_1} are anti-correlated, $\sigma_{T_{GRUAN}(P)}$ is lower than in case 1., i.e.

$$\sigma_{T_{GRUAN}(P)} = \sqrt{\sigma_{T_0}^2 \cdot \left(\frac{\partial T(P)}{\partial T_0}\right)^2 + \sigma_{T_1}^2 \cdot \left(\frac{\partial T(P)}{\partial T_1}\right)^2 - 2\cdot\sigma_{T0}\cdot\sigma_{T1} \cdot \left(\frac{\partial T(P)}{\partial T_0}\right)\cdot\left(\frac{\partial T(P)}{\partial T_1}\right)} = |(1-\beta)\cdot\sigma_{T_0} - \beta\cdot\sigma_{T_1}| \tag{6.5}$$

   The uncertainty in $T(P)$ can become very small if the uncertainties on T_0 and T_1 are anti-correlated. In particular, $\sigma_{T_{GRUAN}(P)} = 0$ for $\beta = \sigma_{T_0}/(\sigma_{T_1} - \sigma_{T_0})$.

3. Completely positively correlated uncertainties ($R = 1$):

If σ_{T_0} and σ_{T_1} are completely positively correlated, $\sigma_{T_{GRUAN}(P)}$ is calculated as a linear interpolation of the temperature uncertainties in logarithmic pressure.

$$\sigma_{T_{GRUAN}(P)} = \sqrt{\sigma_{T_0}^2 \cdot \left(\frac{\partial T(P)}{\partial T_0}\right)^2 + \sigma_{T_1}^2 \cdot \left(\frac{\partial T(P)}{\partial T_1}\right)^2 + 2 \cdot \sigma_{T0} \cdot \sigma_{T1} \cdot \left(\frac{\partial T(P)}{\partial T_0}\right) \cdot \left(\frac{\partial T(P)}{\partial T_1}\right)} = \sigma_{T_0} \cdot (1-\beta) + \sigma_{T_1} \cdot \beta \tag{6.6}$$

For this study we assume the uncertainties on T_1 and T_2 to be fully positive correlated. While this might slightly overestimate the uncertainties (as σ_{T_1} and σ_{T_2} are unlikely to be completely positively correlated), it is currently the best estimate of the uncertainty. If the error covariances are made available for the GRUAN data product at some time in the future, it would be possible to improve the estimate of the uncertainty.

6.1.2 Calculation of background departures (O-Bs)

The departures of the Met Office UM temperatures from the GRUAN temperatures are calculated as:

$$OB = T_{GRUAN} - T_{background} \tag{6.7}$$

The model uncertainty is assumed to be zero as the model is only used as a transfer medium, i.e. the central assumption is that the model bias is constant over the distance between the GRUAN and RO profiles. Thus, the uncertainty on the departures equals the uncertainty on T_{GRUAN}.

$$\sigma_{OB} = \sigma_{T_{GRUAN}} \tag{6.8}$$

Propagating the GRUAN uncertainty through the calculations results in a profile of uncertainties associated with each departure profile.

6.1.3 Calculation of mean GRUAN temperature departures

Following Bevington and Robinson [4], the mean GRUAN temperature departure is calculated as a weighted average, where the weights are determined by the uncertainties on the individual temperature departures σ_{OB} as:

$$\overline{OB} = \frac{\sum_{i=1}^{N} \frac{1}{\sigma_{OB_i}^2} \cdot OB_i}{\sum_{i=1}^{N} \frac{1}{\sigma_{OB_i}^2}} \tag{6.9}$$

The uncertainty of the weighted mean is calculated as (see Bevington and Robinson [4]) :

$$\sigma_{\overline{OB}} = \sqrt{\frac{1}{\sum_{i=1}^{N} \frac{1}{\sigma_{OB_i}^2}} \cdot \frac{1}{N-1} \sum_{i=1}^{N} \frac{(OB_i - \overline{OB})^2}{\sigma_{OB_i}^2}} \tag{6.10}$$

taking into account the standard deviation of the departures, the sample size and the weights, which are determined by the GRUAN uncertainties.

6.2 Analysing the structural uncertainty in RO retrievals at GRUAN sites

In this section, the RO Tdry departures calculated from the COSMIC BA departures around the GRUAN sites are shown for different upper cut-off impact heights. Within this project, an impact height cut-off at 35km is used to analyse the difference between RO and GRUAN O-B departures, but reasonable variations in the upper cut-off impact height would be conceivable. The figures 6.1-6.6 show the Tdry departures for cut-off impact heights of 25 km, 27.6 km, 30 km, 32.6 km, 35 km, 37.6 km, 40 km and 42.6 km. While the spread between departures stays below ~ 0.1 K at some stations (i.e. Barrow, Ny Ålesund) it is larger at others, reaching ~ 0.25 K at 10 hPa. A cut-off close to the altitude of the balloon burst is needed to use the double differencing method which relies on the assumption of a constant model bias over the separation distance between the measurements. However, choosing a cut-off impact height adds structural uncertainty as the O-B statistics depend on the choice. While using a cut-off at 35 km seems to be a reasonable choice within this project, cutting off at 30 km or 40 km could also be adequate. Therefore the range (maximum minus minimum value) of the Tdry departures with cut-offs between 30 km and 40 km impact height is used to estimate the structural uncertainty of the Tdry departure. A general discussion of the structural uncertainty induced by the cut-off and a comparison to the structural uncertainty in the conventional RO retrieval, is given in chapter 5. Based on the burst altitudes of balloons launched at GRUAN sites, it seems to be reasonable to choose cut-off impact heights between 30 km and 40 km to estimate the structural uncertainty. Recall that it is important to use a cut-off impact height approximately coincident with burst point altitude of the RSs. If the cut-off impact height is chosen too low, it precludes the calculation of RO Tdry departures at the highest level where GRUAN departures are available. On the other hand side, choosing a cut-off impact height above the altitude that is reached by the RSs, results in the downward propagation of model biases in the RO retrieval (see Burrows and Healy [6]), invalidating the central assumption needed for double differencing.

In general, it would be possible to choose a station-dependent upper impact height cut-off for GRUAN stations. This would allow the average burst altitude of RSs to be taken into account. For example, the majority of the RSs launched in Lindenberg reach 10 hPa, while this is exceptional for the Southern Great Plains site. The structural uncertainty could then be estimated by variation of this station dependent cut-off impact height. This improvement could be facilitated in a future extension of this study.

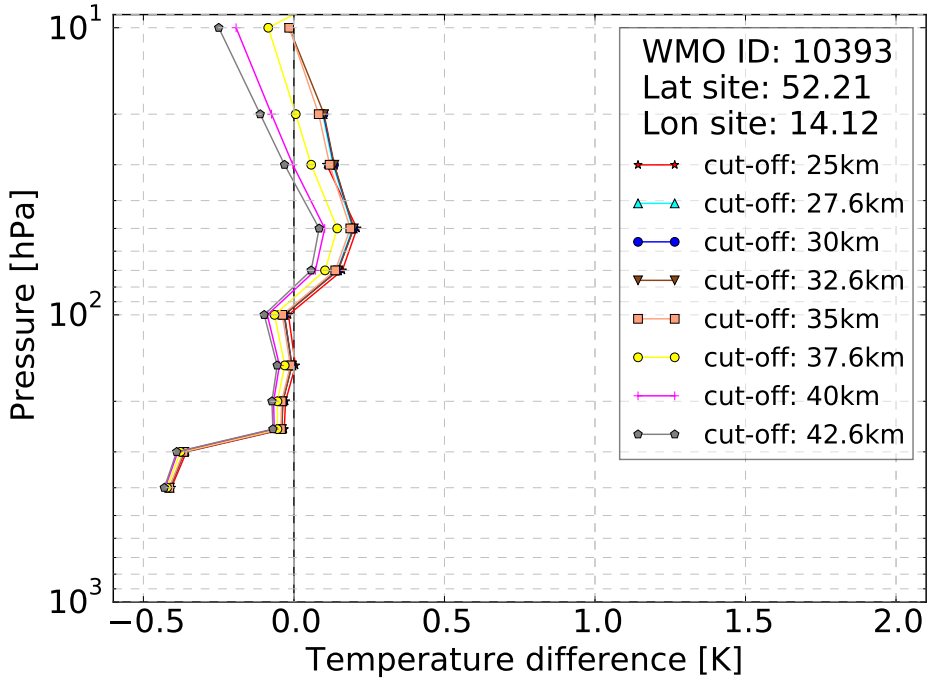

Figure 6.1: *Sensitivity to the upper cut-off impact height at the GRUAN station in Lindenberg.*

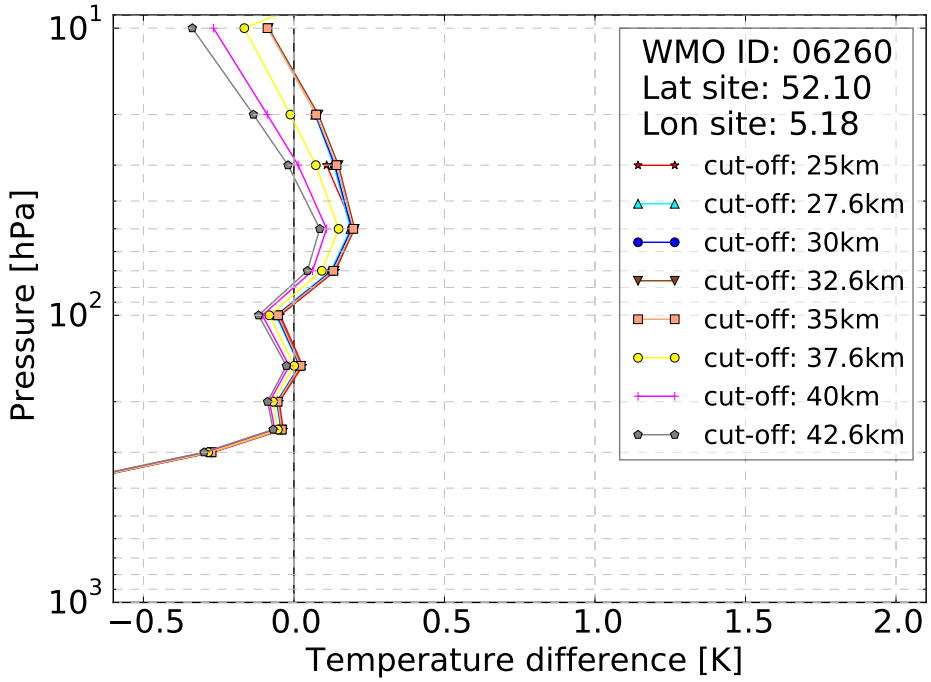

Figure 6.2: *Sensitivity to the upper cut-off impact height at the GRUAN station in Cabauw.*

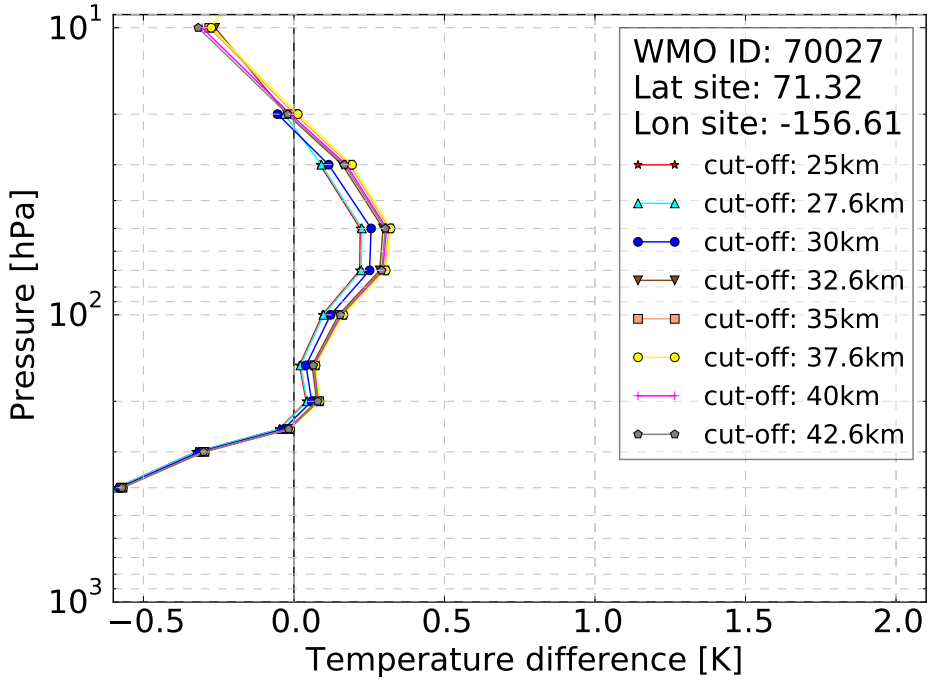

Figure 6.3: *Sensitivity to the upper cut-off impact height at the GRUAN station in Barrow.*

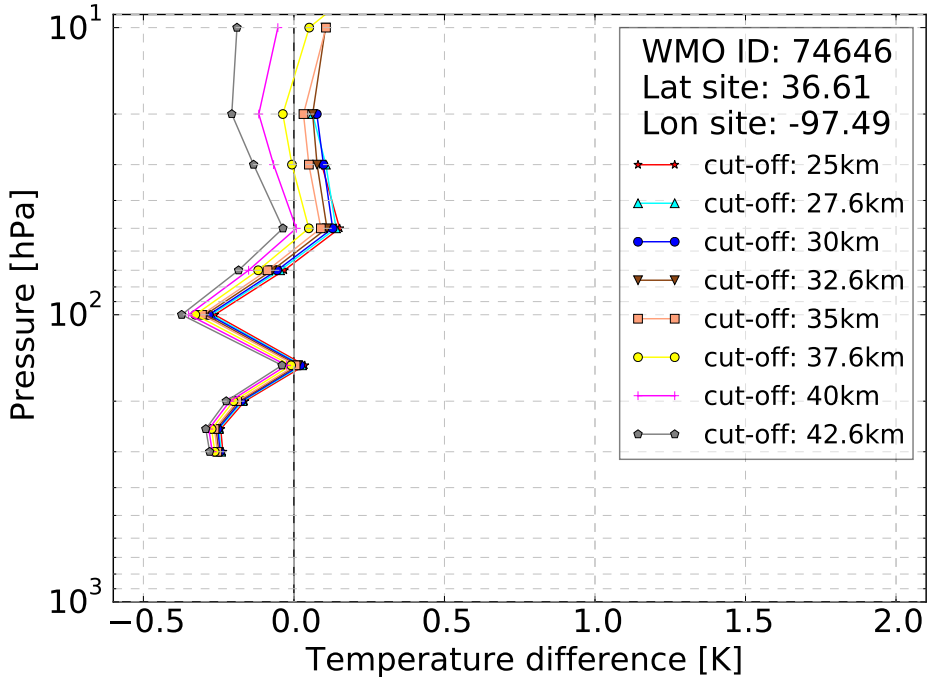

Figure 6.4: *Sensitivity to the upper cut-off impact height at the GRUAN station Southern Great Plains.*

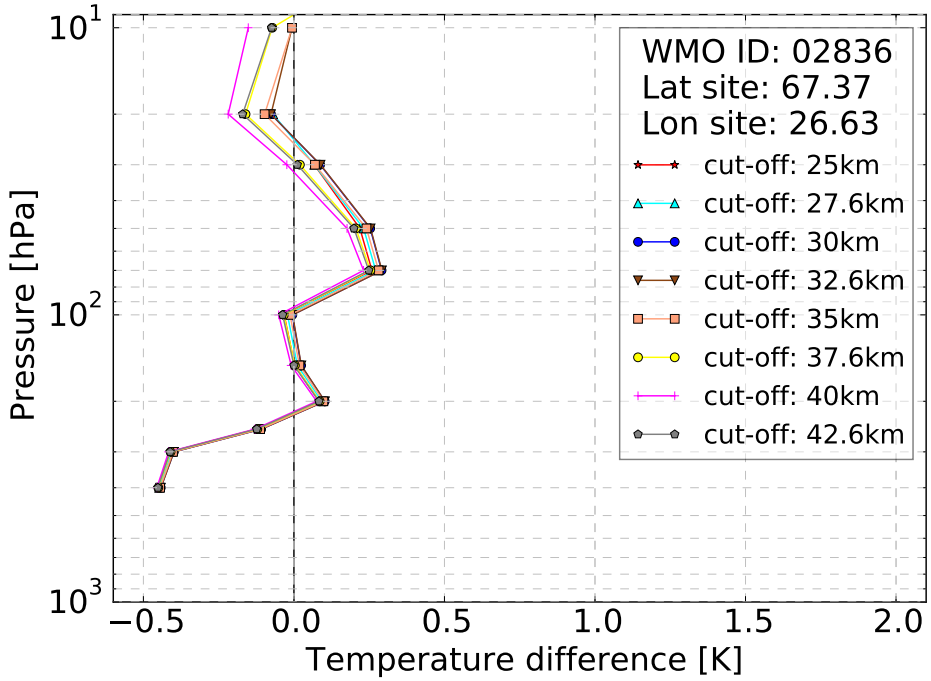

Figure 6.5: *Sensitivity to the upper cut-off impact height at the GRUAN station in Sodankylä.*

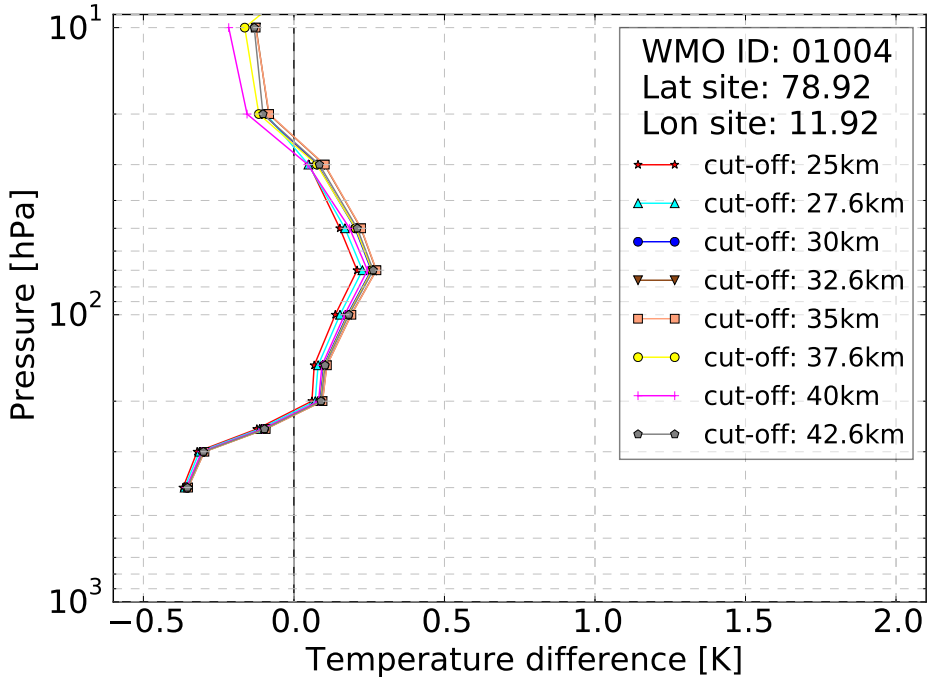

Figure 6.6: *Sensitivity to the upper cut-off impact height at the GRUAN station in Ny Ålesund.*

6.3 Comparison of GRUAN and RO departure statistics

In this section, the GRUAN departures are compared to RO departures and the differences are analysed. As GRUAN is offering data products accounting for all known systematic biases, and RO measurements are known to have a high accuracy in the upper troposphere and lower stratosphere, the expectation is that the data are mostly either consistent or in agreement. Using temporal and spatial co-locations (3 hours and 300 km), Ladstädter et al. [24] found a warm bias in GRUAN measurements at high altitudes, with good agreement otherwise. Using the method applied here, a comparison of RO BAs propagated into Tdry space and GRUAN temperatures is possible at altitudes above ~150 hPa. At lower altitudes, Tdry is not a valid estimate of the temperature due to the effects of humidity. As for the RS statistics, the highest pressure level at which the comparison can be made is shown with a cyan coloured horizontal line in Figs. 6.8-6.26. At altitudes below this line the number of RO profiles decreases, and those RO profiles that are included are sampled in especially dry airmasses.

In the context of GRUAN, consistency between two independent measurements is achieved if

$$|m_1 - m_2| < k \cdot \sqrt{u_1^2 + u_2^2} \tag{6.11}$$

is true for k=1 (Immler et al. [19]). k is the coverage factor "which determines an interval about the mean value as a multiple of standard uncertainty" (Immler et al. [19]). If Eq.6.11 is true for $k = 2$ the data are in statistical agreement. The $k = 1$ uncertainty is plotted as the error bars on the difference (RO O-B minus GRUAN O-B). Thus, if the uncertainty range in Figs.6.7,6.10,6.13,6.16,6.19,6.22 comprises the vertical zero difference line, the GRUAN and RO temperatures are consistent at a given pressure level.
For every analysed GRUAN station, it is tested if the GRUAN O-Bs and RO O-Bs are consist or in agreement. If they are not in agreement (i.e. if $|m_1 - m_2| > 2 \cdot \sqrt{u_1^2 + u_2^2}$) potential reasons are discussed.

In the following subsections, the O-B statistics of GRUAN and RO are discussed for those GRUAN sites that have a sufficient sample size of profiles to calculate valid statistics. For every station, three plots are shown, as explained below:

1. The Figs.6.8,6.11,6.14,6.17,6.20,6.23 show the GRUAN departures in pink, the RO Tdry departures in blue and the difference between the RO O-B and GRUAN O-B in green. The dashed lines give the RO (blue) and GRUAN (pink) sample size. The horizontal cyan line indicates the highest standard pressure level (lowest altitude) where at least 95% of the RO profiles are included. The RO uncertainty bars represent the standard errors (sampling uncertainty) calculated as $SE = \sigma / \sqrt{(n-1)}$. The GRUAN uncertainty bars are calculated as explained in section 6.1.3. The uncertainty bars on RO O-B minus GRUAN O-B are $SE_{difference} = \sqrt{SE_{RO}^2 + SE_{GRUAN}^2}$.
2. The Figs.6.7,6.10,6.13,6.16,6.19,6.22 show the same departure statistics as the figures explained above, but the RO uncertainty bars include the sampling plus the structural uncertainty. The structural uncertainty is calculated as the range of the departures between 30 km and 40 km divided by two. Thus, the updated RO uncertainty is calculated as $uncertainty_{RO} = SE + range/2$. The uncertainty bars on RO O-B minus GRUAN O-

B are calculated as $SE_{difference} = \sqrt{uncertainty_{RO}^2 + SE_{GRUAN}^2}$.
In the following sections these figures including both, structural and sampling uncertainty are discussed. The other figures are only included to offer the possibility to separate the sampling and structural uncertainty estimate.

3. The Figs.6.9, 6.12, 6.15, 6.18, 6.21, 6.24 the uncertainty on the differences between the RO and GRUAN departures is shown for $k = 1$ (consistency, red) and $k = 2$ (agreement, red dashed). If the absolute value of the RO O-B minus GRUAN O-B (green) is lower than the threshold for consistency (agreement), the GRUAN departures are consistent (in agreement) with the RO departures.

6.3.1 Lindenberg, Germany

The GRUAN station in Lindenberg, Germany, is operated by *Deutscher Wetterdienst*, the German weather service and is situated at the GRUAN Lead-Centre. Radiosondes are launched four times daily and the Vaisala RS product is submitted to the GTS regularly.

In Fig.6.7 the RO and GRUAN departures are consistent at most levels for high and low SEA (Fig.6.7(a)) from 150 hPa to 20 hPa. At the highest altitude (lowest pressure level) a negative difference between RO O-B and GRUAN O-B exists, implying that the GRUAN temperature is nearly 0.5 K warmer at this level. This agrees with the results from Ladstädter et al. [24], who found that GRUAN temperatures are slightly warmer than RO Tdry retrievals from the Wegener Center for Climate and Global Change. For dusk/dawn (Fig.6.7(c)) and night (Fig.6.7(d)) the RO O-B minus GRUAN O-B profile is mostly slightly positive, with consistency at some levels. As a comparison can only be performed if a sufficient amount of RO profiles sampled in dry conditions is available, all data below the cyan coloured line are not discussed here.

For high SEA consistency or agreement is found at all but the very highest altitude (see Fig.6.9). For low SEA all levels show consistency or agreement. For dusk/dawn and night SEAs the GRUAN and RO departures are inconsistent at the 70 hPa or 70-50 hPa level respectively. The reason for the inconsistencies is not known.

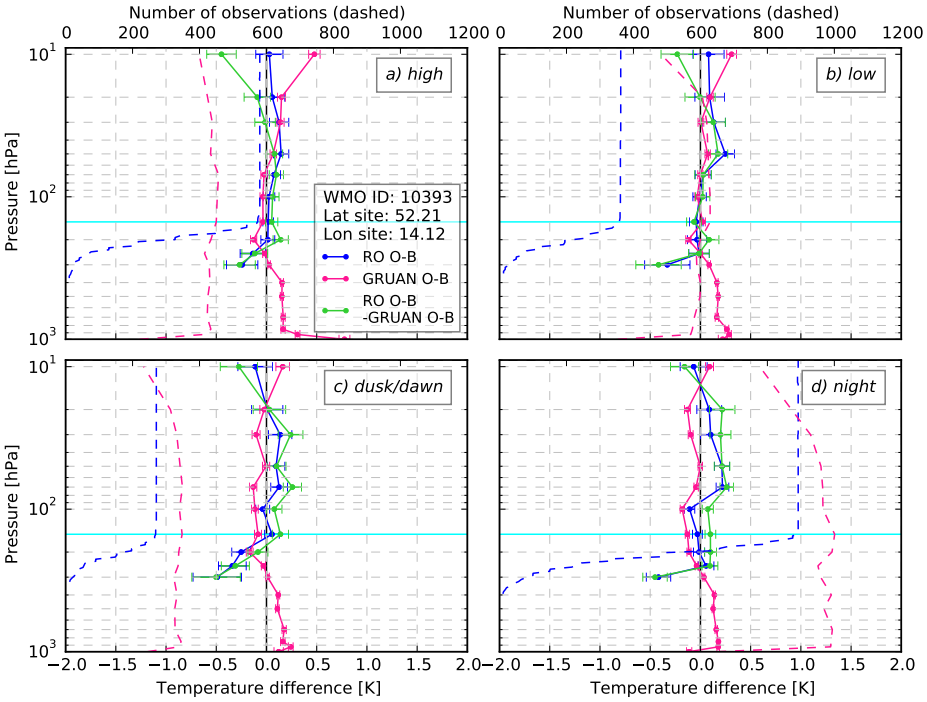

Figure 6.7: *Mean RO Tdry departures (blue), mean GRUAN temperature departures (pink) and RO O-B minus GRUAN O-B (green) at the GRUAN site in Germany for different SEA ranges (a)-(d). The horizontal cyan line indicates the highest standard pressure level (lowest altitude) where at least 95% of the RO profiles are included. The RO error bars represent the structural uncertainty in addition to the sampling uncertainty, i.e. uncertainty* $= SE + range/2$.

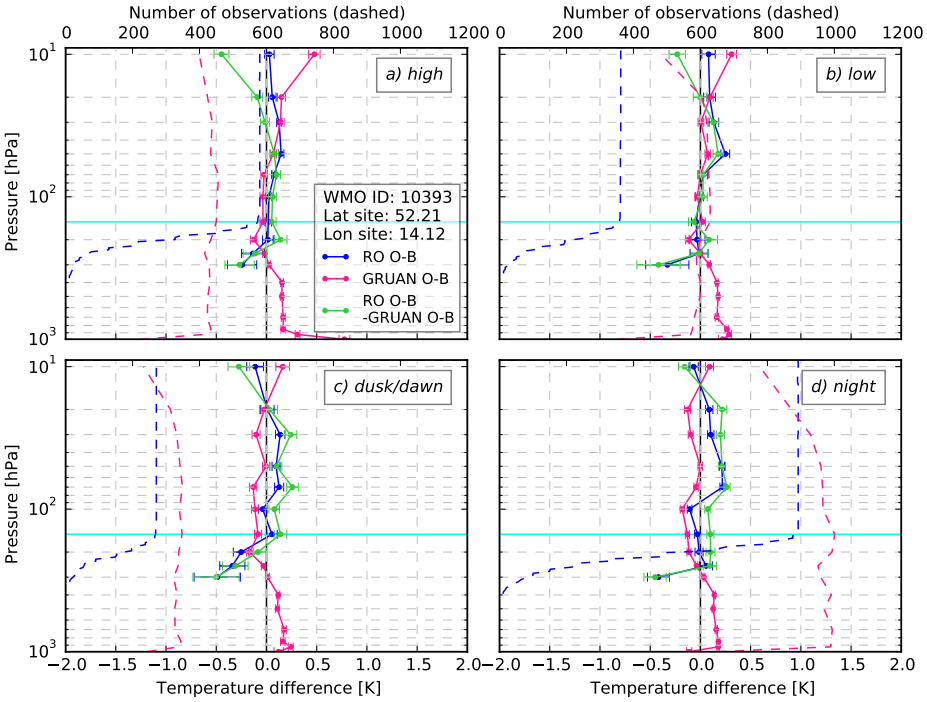

Figure 6.8: *Mean RO Tdry departures (blue), mean GRUAN temperature departures (pink) and RO O-B minus GRUAN O-B (green) at the GRUAN site in Germany for different SEA ranges (a)-(d). The horizontal cyan line indicates the highest standard pressure level (lowest altitude) where at least 95% of the RO profiles are included. The RO error bars represent the standard errors (sampling uncertainty) calculated as* $SE = \sigma / \sqrt{(n-1)}$.

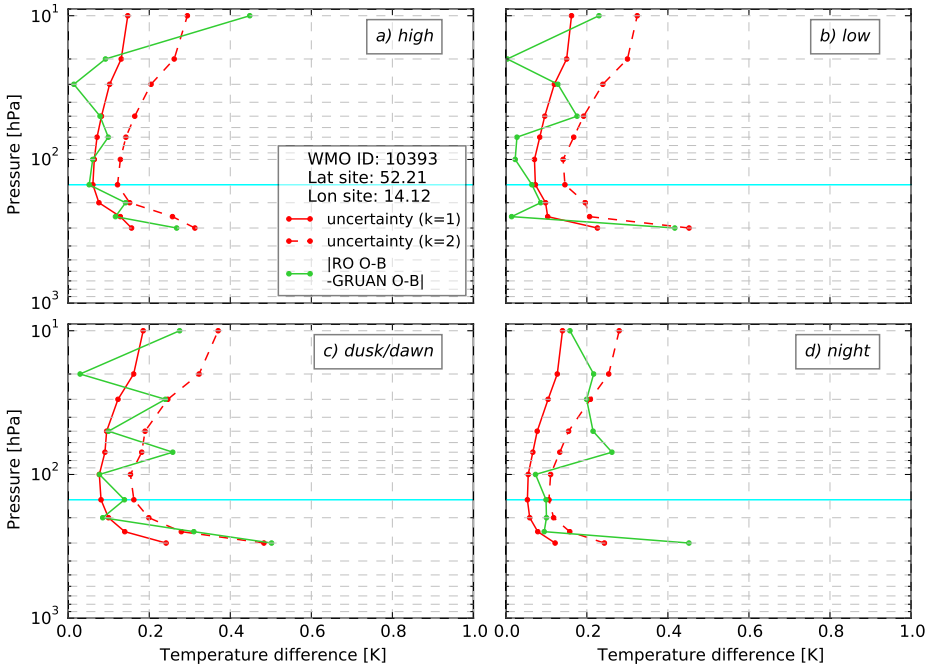

Figure 6.9: *Uncertainties of RO O-B minus GRUAN O-B for $k = 1$ (red) and $k = 2$ (red dashed) and the absolute value of RO O-B minus GRUAN O-B (green). Statistics are presented for the GRUAN site in Germany for different SEA ranges (a)-(d). The horizontal cyan line indicates the highest standard pressure level (lowest altitude) where at least 95% of the RO profiles are included.*

6.3.2 Cabauw, Netherlands

The measurement station Cabauw/De Bilt in the Netherlands is operated by the Dutch Weather Service *Koninklijk Nederlands Meteorologisch Instituut* (KNMI). During 2016 Cabauw was the 8^{th} upper-air site that received formal certification for its GRUAN radiosonde operations.

494 GRUAN profiles are available for the upper-air site in De Bilt during 2014 and 2015, with most launches performed during night-time. For high and low SEAs the GRUAN and RO departures presented in Fig.6.10(a),(b) are consistent for most pressure levels between 150 hPa and 20 hPa. At 10 hPa they are not consistent and the difference between the departures is negative. As the GRUAN sample size for high and low SEAs is small, the results might not be robust. The RO and GRUAN departures are inconsistent at all pressure levels for night-time launches (Fig. 6.10(d)). Figure 6.12 shows that agreement is found at 150 hPa and at 30 hPa, but statistical significant differences or inconsistencies (following Immler et al. [19]) are found at all other levels. The GRUAN sample size is decreasing at pressures below 70 hPa and thus a sampling bias might be present in the statistics. This is caused by the dependence of the burst altitude on the atmospheric parameters, e.g. humidity or temperature. Thus the decreasing amount of GRUAN data at high altitudes might include preferential sampling in specific conditions. As the RO profiles are sampled in all atmospheric conditions, the double differencing method might not offer a valid estimation of the differences between the RO and GRUAN departures if a GRUAN sampling bias at high altitudes is present.

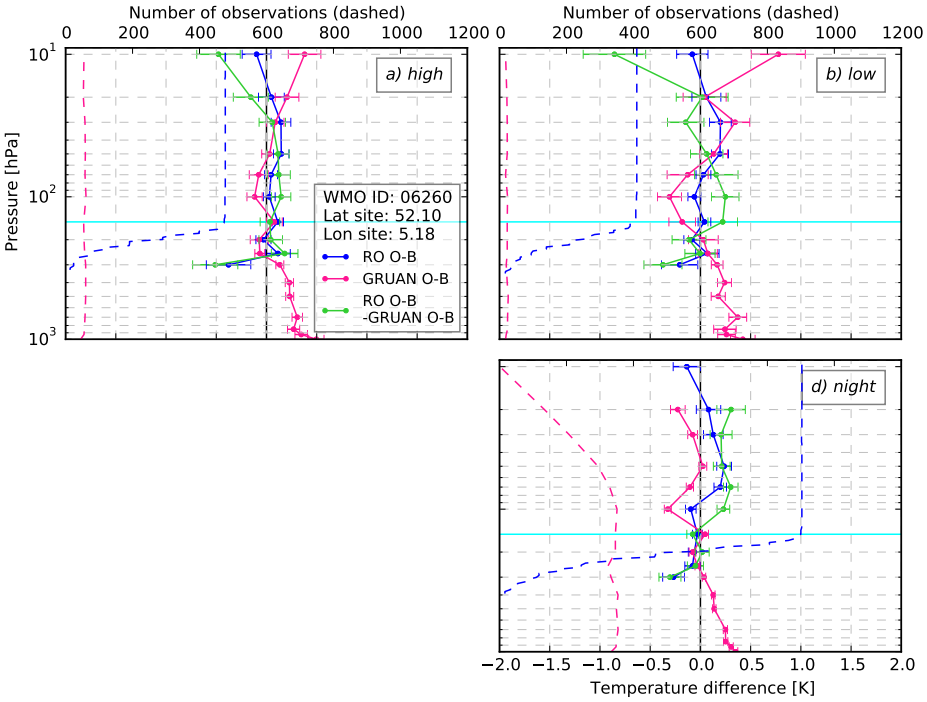

Figure 6.10: *As in Fig.6.7, but for the GRUAN site Cabauw.*

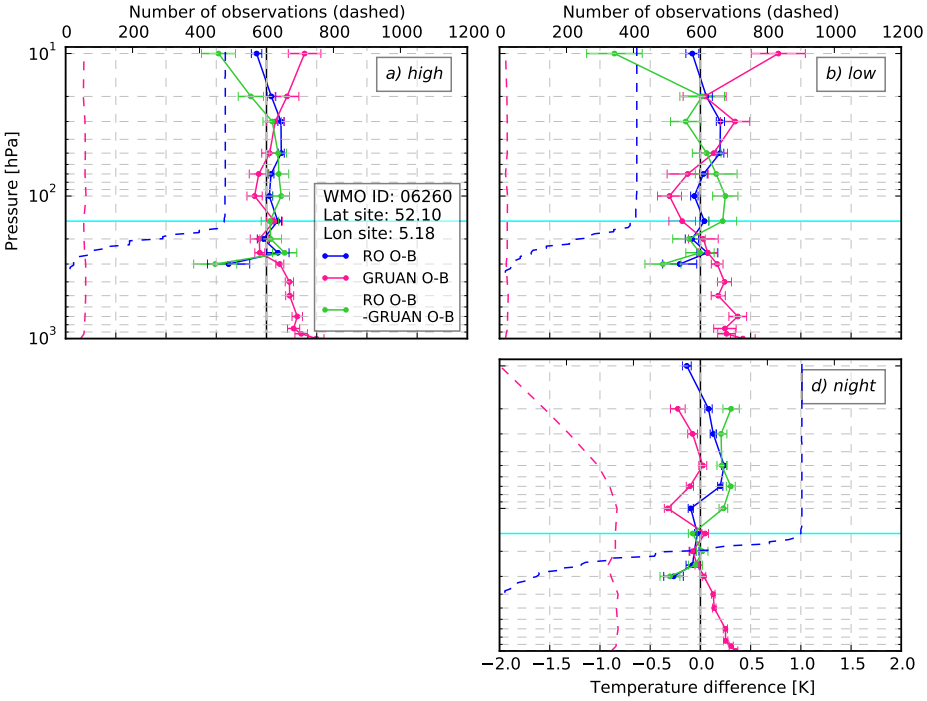

Figure 6.11: *As in Fig.6.8, but for the GRUAN site Cabauw.*

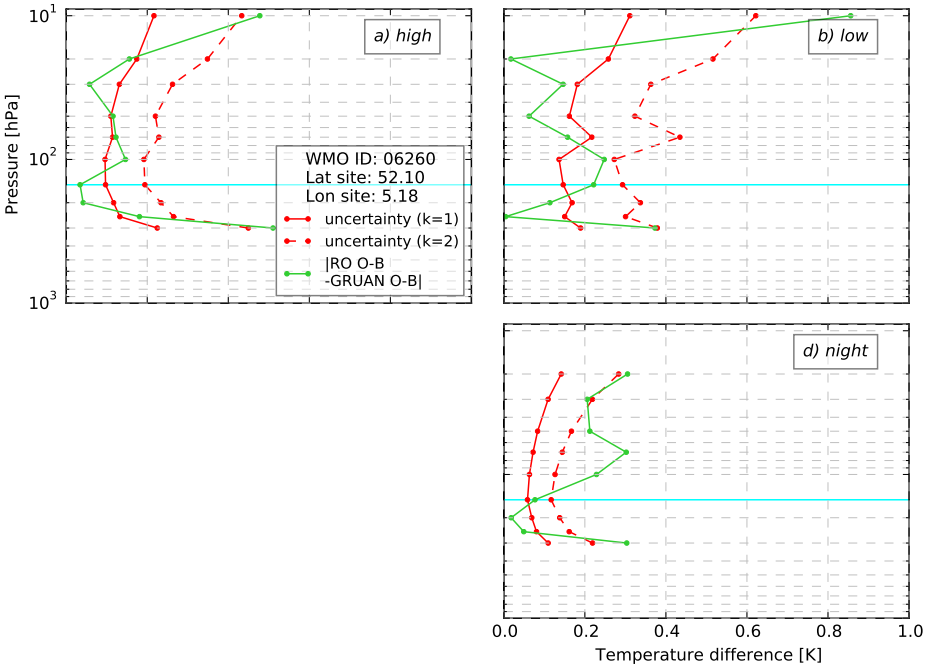

Figure 6.12: *As in Fig.6.9, but for the GRUAN site Cabauw.*

6.3.3 Barrow, Alaska, United States

The GRUAN site in Barrow, Alaska is operated by the US *Department of Energy* as part of the *Atmospheric Radiation Measurement* program. More than 100 GRUAN profiles are available per SEA range, though most of them do not reach 10 hPa. For high and low SEA ranges (see Fig.6.13(a),(b)), the RO and GRUAN departures are consistent at all pressure levels between 150 hPa and 30 hPa. At the 20 hPa level, the GRUAN sample size is minimal and thus the results at this level are unreliable.

At dusk/dawn the GRUAN and RO departures are consistent at all but the 100 hPa level, where they are statistically significant different (see Fig.6.13(c) and Fig.6.15(c)). At night-time the GRUAN and RO departures are in agreement at some levels, but show statistically significant differences at others (see Fig.6.15(d)).

At the majority of pressure levels, RO and GRUAN departures from model background are more similar to each other than the magnitude of their value, i.e. RO and RS are closer to each other than either is to the model background. This indicates an error in the model. Similar behaviour is also be found at some other stations, but to a varying extend.

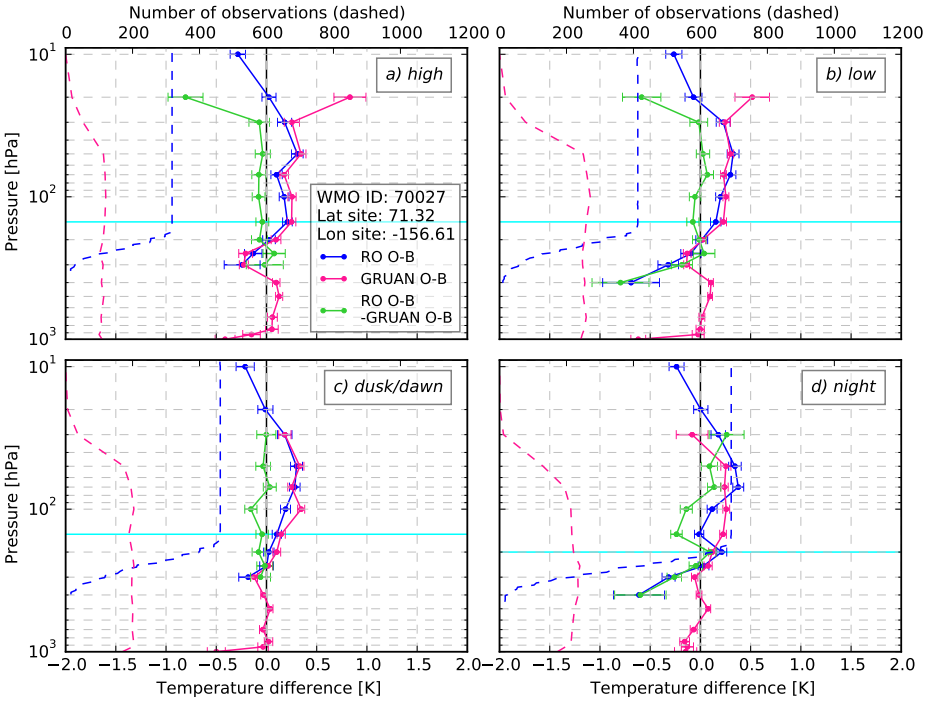

Figure 6.13: *As in Fig.6.7, but for the GRUAN site Barrow.*

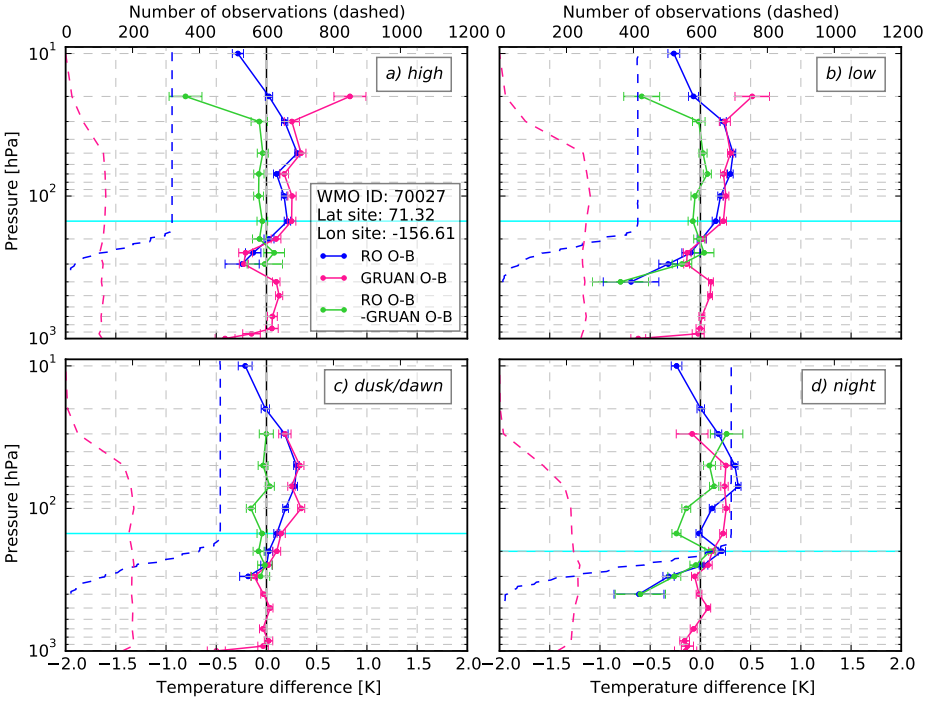

Figure 6.14: *As in Fig.6.8, but for the GRUAN site Barrow.*

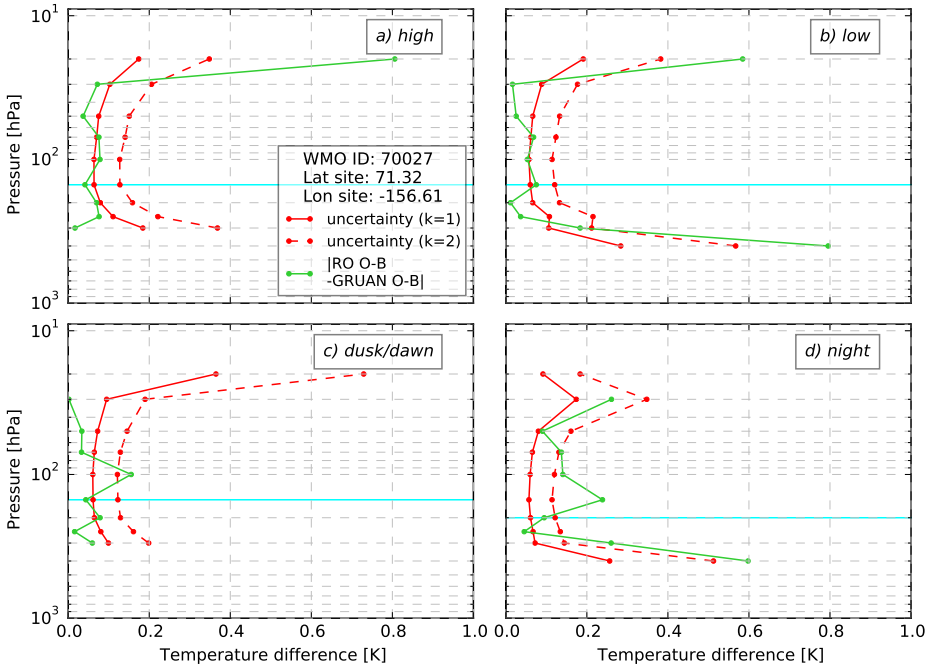

Figure 6.15: *As in Fig.6.9, but for the GRUAN site Barrow.*

6.3.4 Southern Great Plains, Kansas, United States

The GRUAN site Southern Great Plains in Lamont, Kansas is a super-site operated by the US *Department of Energy* as part of the *Atmospheric Radiation Measurement* program.

Compared to the other sites, larger differences between the RO and GRUAN O-Bs are found at the Southern Great Plains site. The pressure range in which enough RO and GRUAN profiles are available is comparably small, as the amount of GRUAN profiles is decreasing at pressures below approximately 50 hPa and a sufficient RO sample size is only available starting from 100 hPa.

For high, low and dusk/dawn launches (Fig.6.18(a)-(c)) agreement is found at some levels, while the RO and GRUAN departures are statistically significant different at other levels. For night-time launches (Fig.6.18(d)), statistical significant differences are found at all levels. The reason for the lack of consistency/agreement between the GRUAN and RO departures at this specific site is not clear. As the RS launched at this site do commonly not reach the 10 hPa level, the choice of a lower cut-off impact height would be conceivable. The RO O-B profile for a cut-off impact height of 25 km at the Southern Great Plains site is though similar to the the profile calculated with a cut-off at 35km as can be seen in Fig.6.4. Thus, lowering the cut-off impact height would not result in major changes.

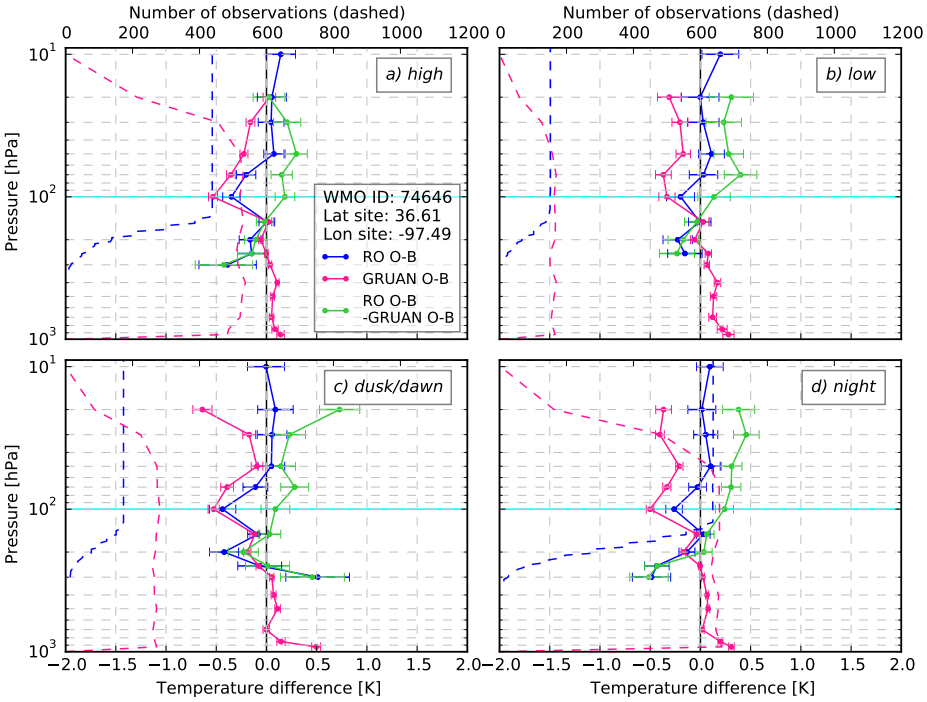

Figure 6.16: *As in Fig.6.7, but for the GRUAN Southern Great Plains site.*

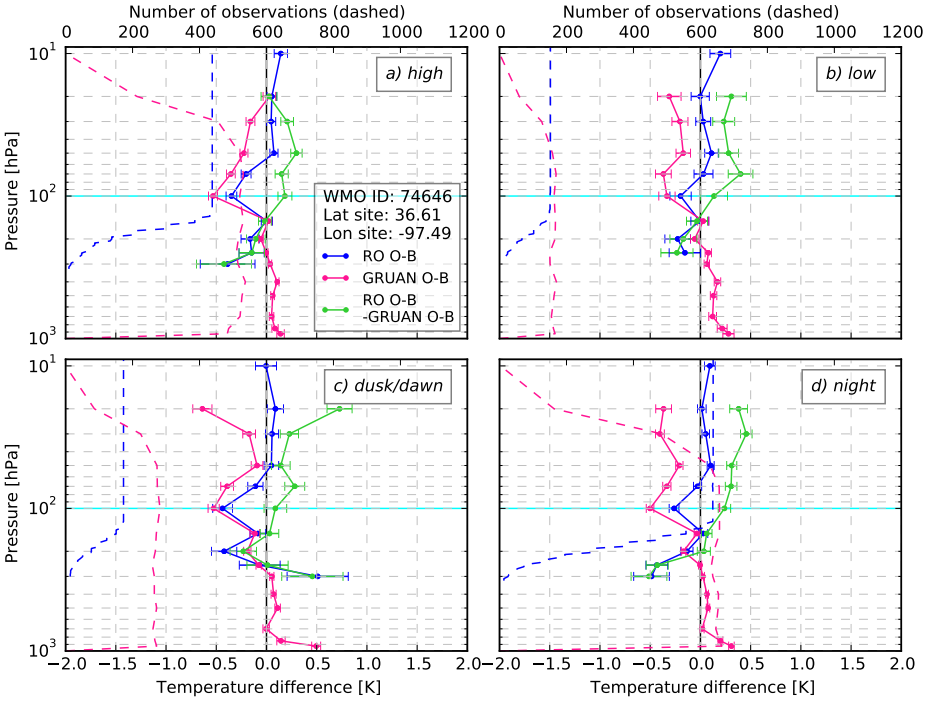

Figure 6.17: *As in Fig.6.8, but for the GRUAN Southern Great Plains site.*

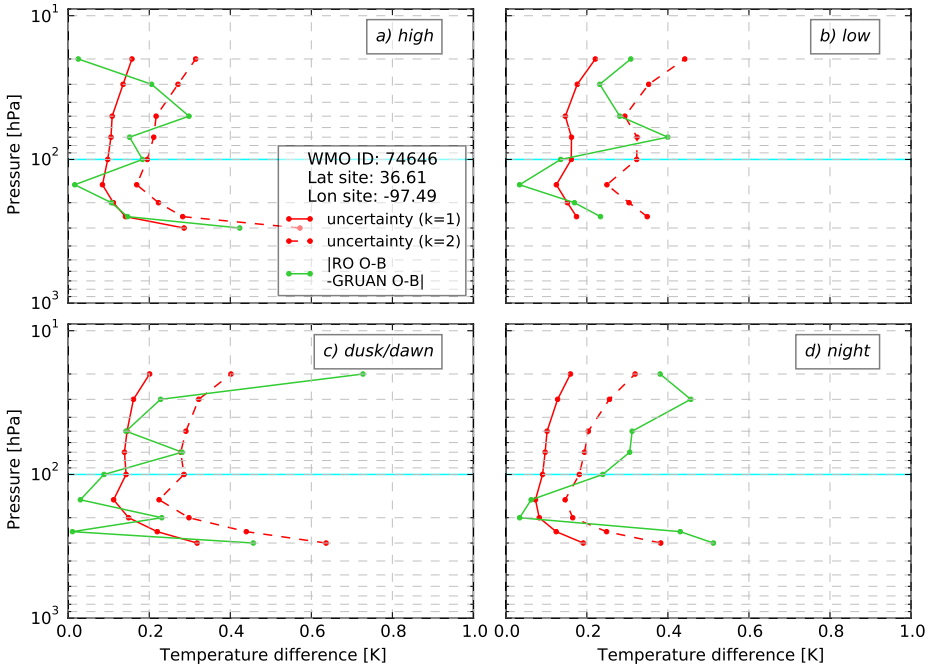

Figure 6.18: *As in Fig.6.9, but for the GRUAN Southern Great Plains site.*

6.3.5 Sodankylä, Finland

The GRUAN site in Sodankylä, Finland is operated by the *Finnish Meteorological Institute*. Most RS launches are performed with an auto launcher, but also some manual launches are included in the GRUAN data set.

For all SEA ranges consistency or agreement is found at all but the 10 hPa level, where the RO O-B minus the GRUAN O-B is consistently negative for all SEA ranges. As the sample size is diminished at the 10 hPa level, a sampling bias for the GRUAN sondes as described in section 6.3.2 might cause the statistically significant differences between the RO and GRUAN departures.

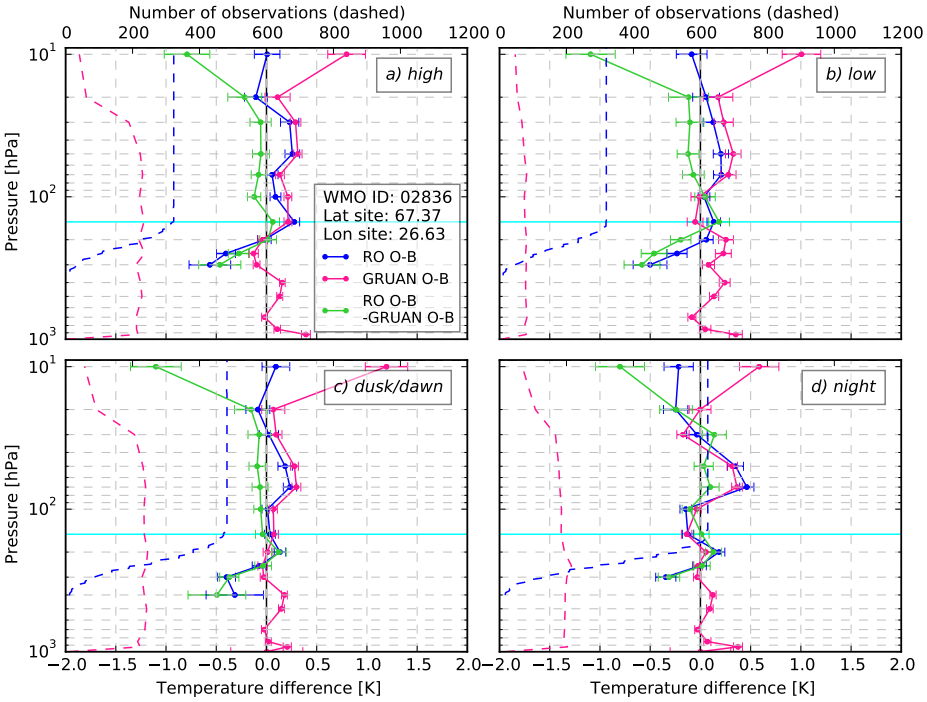

Figure 6.19: *As in Fig.6.7, but for the GRUAN site at Sodankylä.*

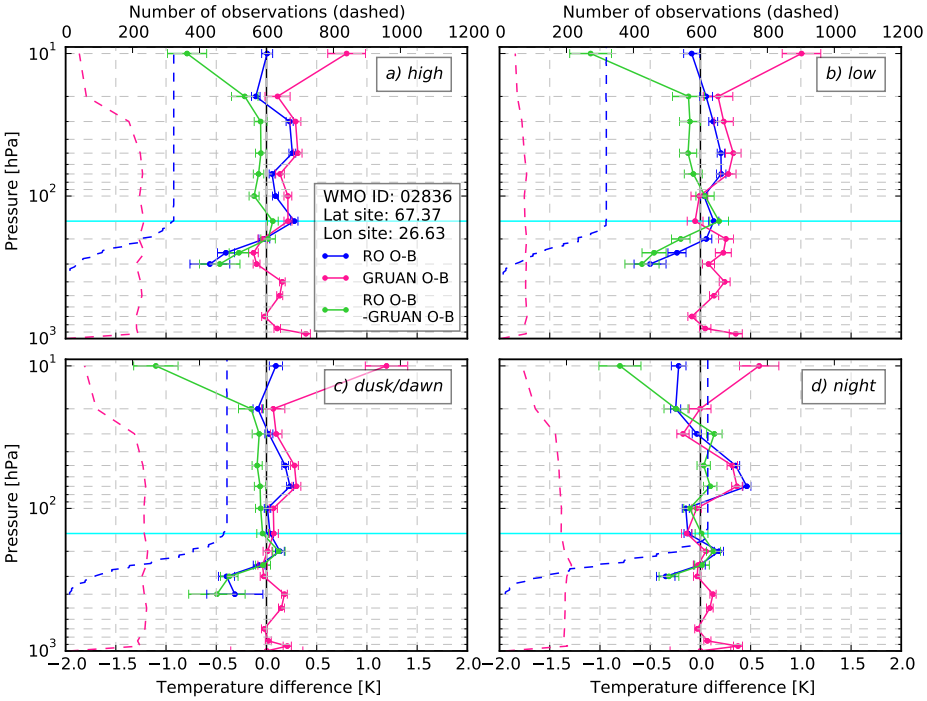

Figure 6.20: *As in Fig.6.8, but for the GRUAN site at Sodankylä.*

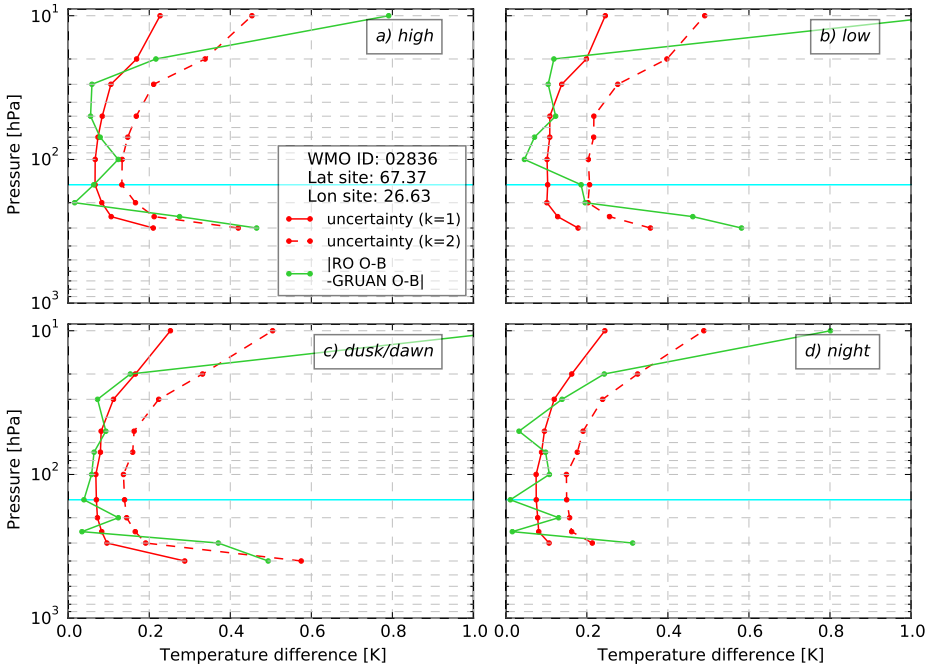

Figure 6.21: *As in Fig.6.9, but for the GRUAN site at Sodankylä.*

6.3.6 Ny Ålesund, Norway

The upper-air site in Ny Ålesund, Svalbart, Norway, at a latitude of 78.92° is the northernmost station within GRUAN. The station is operated by *Alfred-Wegener-Institut* based in Potsdam, Germany.

For all SEAs and most levels with pressure larger than 30 hPa, the GRUAN and RO departures are consistent or in agreement as can be seen in Fig.6.24. But at the top level(s) statistically significant differences are found for all SEA ranges. Here the RO O-B minus GRUAN O-B is without exception negative, which means that the GRUAN temperatures are warmer than the RO implied temperatures. In contrast to situation at Sodankylä, the sample size stays approximately constant up to 10 hPa and thus the differences can not be caused by preferential sampling at certain atmospheric conditions. There are at least two other possible explanations for the significant differences between RO and GRUAN departure statistics at the highest level for all SEA ranges, i.e.

- The proximity to the polar jet, could violate the central assumption of a constant model bias over the separation distance between the RO and RS location. Given that the model bias could vary between the polar jet and the surrounding area, caution needs to be taken when analysing the results. Some RO and GRUAN profiles will be sampled inside and others outside of the polar jet. A quantitative analysis of the implications is not part of this project, but could be a useful extension of this work.
- Preferential sampling of GRUAN profiles in a specific season. RS are launched at specific times of the day (typically a subset of 00 UTC, 6 UTC, 12 UTC, and 18 UTC). These fixed times can lead to preferential sampling during one season, especially in high latitudes, i.e. the dusk/dawn launches could all be made within two months of the year when the standard launch time coincides with dusk or dawn. As the RO departures

are calculated from the RO profiles measured in all seasons, a potentially existing seasonal model bias could influence the results. To investigate the seasonal influence, the departure statistics are calculated separately for the summer and winter half year in section 6.4.

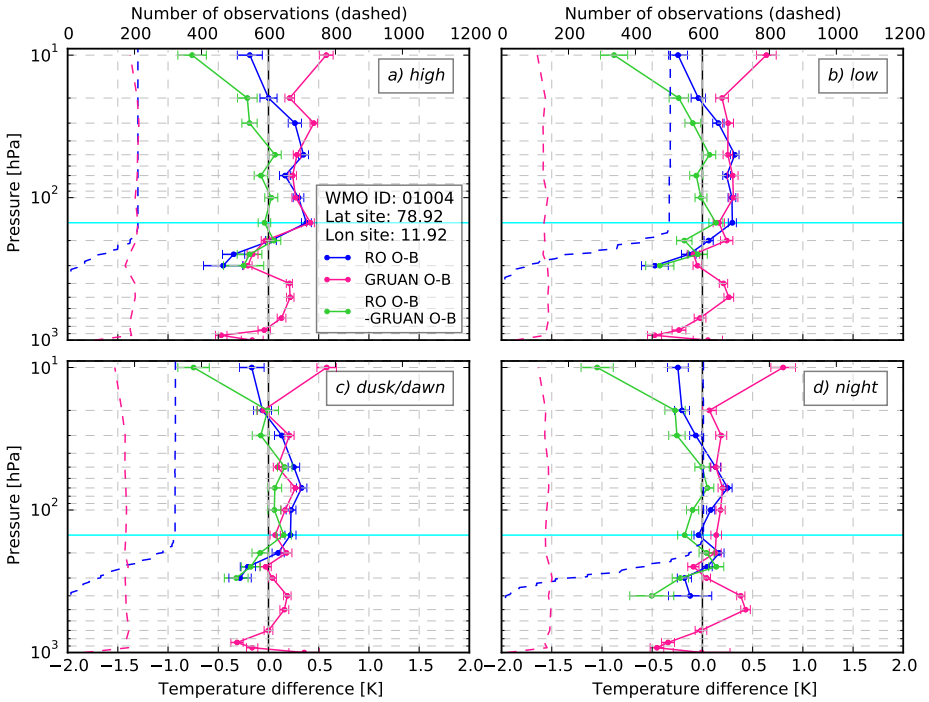

Figure 6.22: *As in Fig.6.7, but for the GRUAN site at Ny Ålesund.*

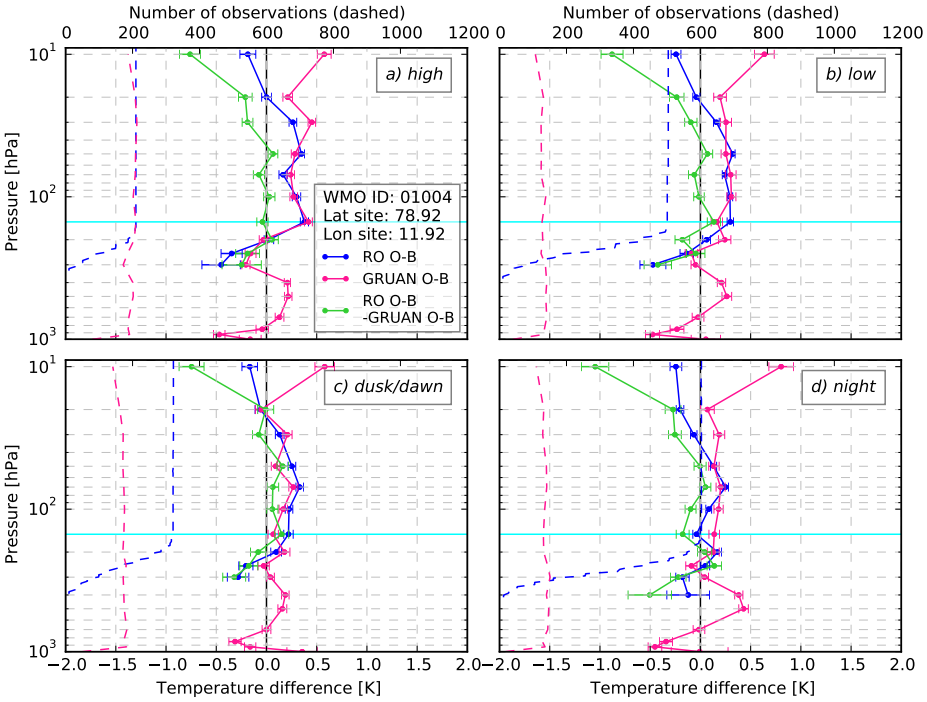

Figure 6.23: *As in Fig.6.8, but for the GRUAN site at Ny Ålesund.*

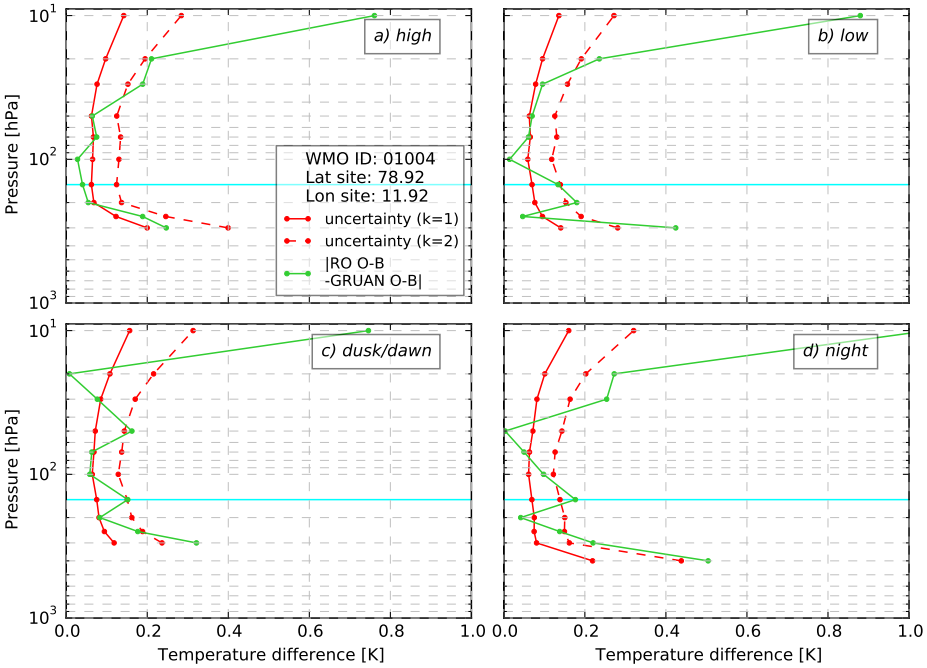

Figure 6.24: *As in Fig.6.9, but for the GRUAN site at Ny Ålesund.*

6.4 Analysis of seasonal dependence for the GRUAN sites at Sodankylä and Ny Ålesund

Especially for those upper-air sites located at high latitudes, it is possible that a seasonal bias in the model propagates into a seasonal bias in the departure statistics. This is caused by the fact that the RSs are launched around standard launch times of 0 UTC, 6 UTC, 12 UTC and 18 UTC. At high latitudes, is is conceivable that all RS measurements within a given SEA range are made during a certain season, while the RO departures include measurements from all/most seasons. This could invalidate the central assumption on which the double differencing technique is based, i.e. the model background bias is constant over the separation distance. This assumption could be invalidated if the model bias has a seasonal dependence. To test if the high altitude difference between GRUAN and RO departures, which is found at all SEA ranges, for the sites at Sodankylä and Ny Ålesund is caused by a seasonal varying model bias, the departures are calculated separately for the summer and winter half year, i.e. for the months April-September (summer half-year) and October-March (winter half-year).

Figure 6.25 shows the departure statistics at Ny Ålesund for the summer half-year (a) and the winter (b) half-year separately. For some SEA ranges the number of profiles available is too small to calculate the departure statistics for a half-year. The statistics for high SEA ranges are calculated only for the summer months and valid night-time departures are only available in winter. The very low GRUAN sample size at low SEA during the winter months precludes a robust statistical analysis. For the dusk/dawn SEA range, better agreement is found during the summer months than for the whole year. Here GRUAN and RO departures are similar at most pressure levels. During the winter months at dusk/dawn, the RO O-B minus GRUAN O-B is ~-0.8 K. Similarly values are also found for the departures calculated from night-time launches performed in winter.

The departure statistics calculated for summer and winter months separately for Sodankylä are shown in Fig.6.26. Unfortunately the number of measurements at the highest level is too low for most SEA ranges to analyse the results. It is clear though, that there are large positive O-Bs for GRUAN in the winter months at the highest levels for all launch times. As discussed in section 6.3.5 the decreasing GRUAN sample at the top levels, could lead to a sampling bias which could cause the large difference between the GRUAN and RO O-B statistics.

Figure 6.26 furthermore indicates that a seasonal model bias between 70 hPa and 50 hPa at the Sodankylä site might exist. During the winter months, both the GRUAN and the RO departures are positive at 70-50 hPa and consistent/in agreement during night-time. This model bias is also apparent for dusk/dawn in the winter months, but with a lesser degree.

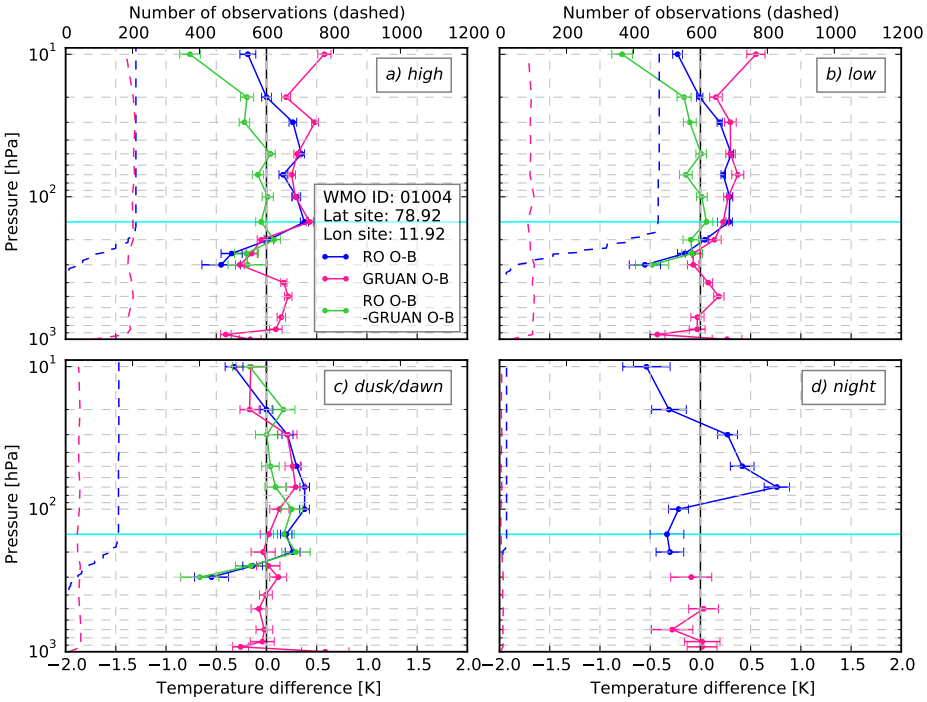

(a) Summer half-year

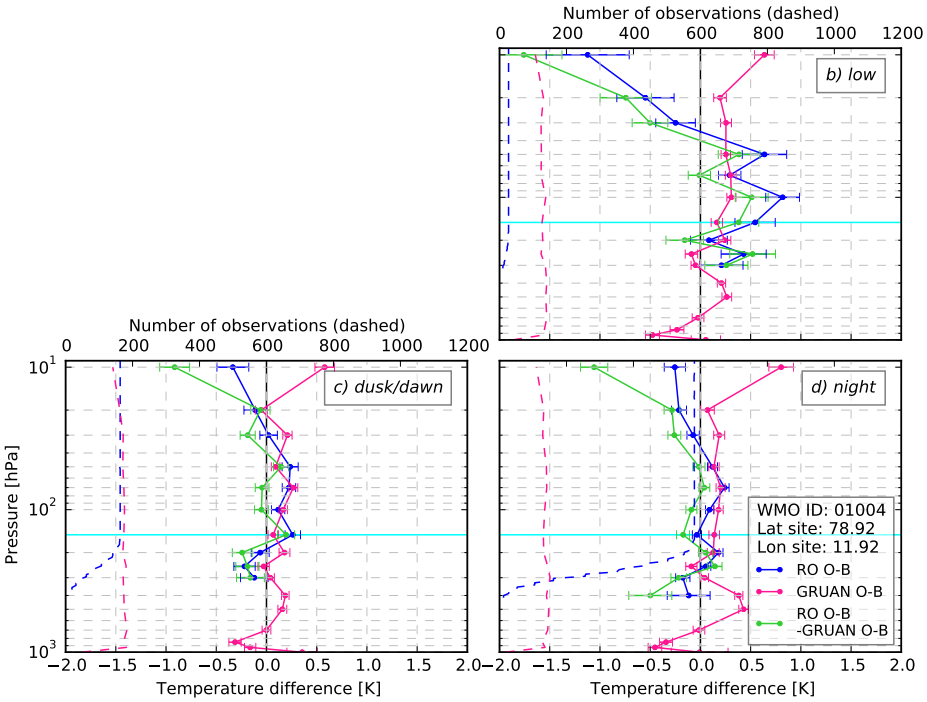

(b) Winter half-year

Figure 6.25: *As in Fig.6.8, but for the GRUAN site at Ny Ålesund. (a) summer half-year, (b) winter half-year.*

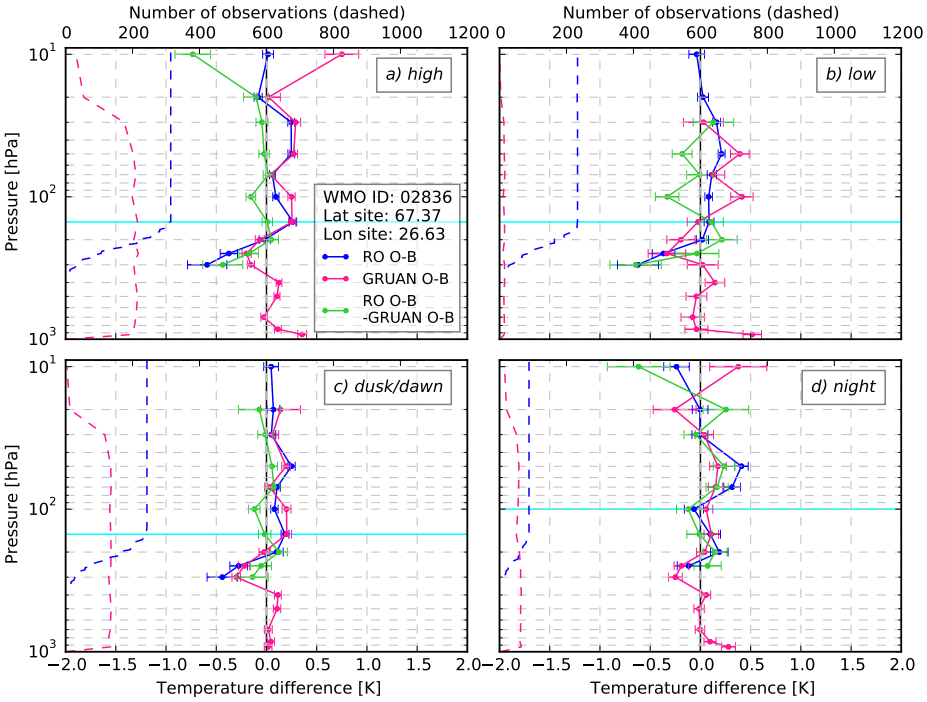

(a) Summer half-year

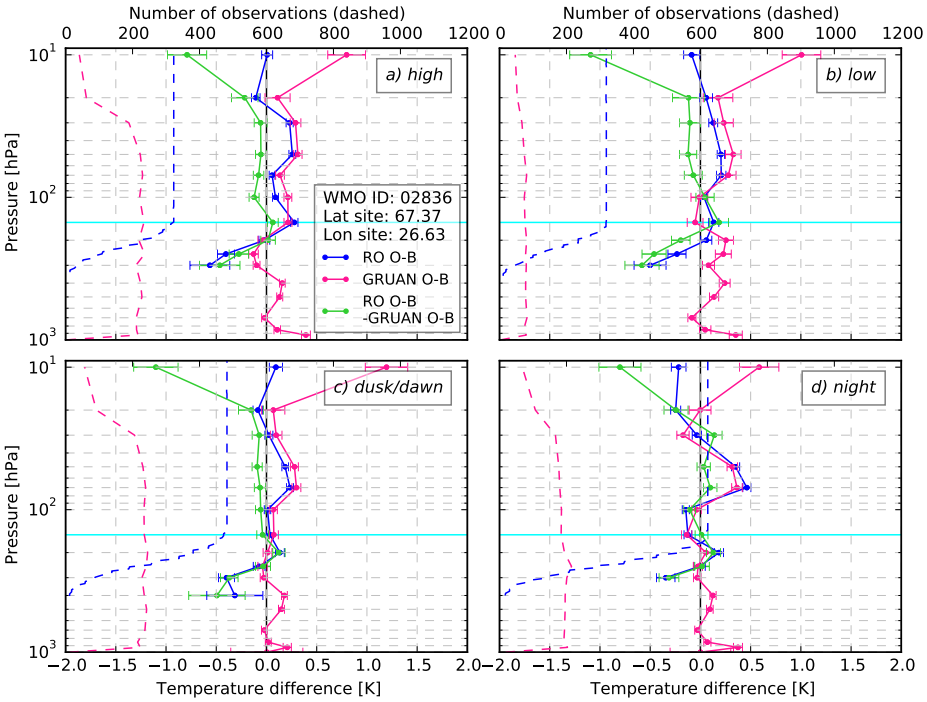

(b) Winter half-year

Figure 6.26: *As in Fig.6.8, but for the GRUAN site at Sodankylä. (a) summer half-year, (b) winter half-year.*

7 Summary and conclusions

The content of this ROM SAF visiting scientist project builds upon the technique and the results presented in the ROM SAF VS26 (Tradowsky [35]), which developed a new method to correct RS temperature biases using RO BAs as unbiased references. The Met Office global NWP system is used as a transfer medium, rather than using co-locations of RO and RS profiles. Within Tradowsky [35] the method was developed, including a tangent linear retrieval to propagate BA departure statistics (i.e. RO observation minus model background) into Tdry departure statistics. Using the method, stratospheric temperature bias corrections were calculated for most upper-air sites, though, the bias correction profiles were not ready to be applied in a forecast impact study. This project aims to further use and analyse the new method and comprises three work packages, i.e.:

- Preparation for a forecast impact study to test the new RS temperature bias correction calculated using the method described in Tradowsky [35].
- Estimation of the structural uncertainty added by choosing an upper cut-off for the BA departures as it is done in the RO retrieval that is used to calculate the RS biases.
- Comparison of the GRUAN temperature departures with RO BA departures propagated into Tdry space.

As a result of this project the RS temperature bias corrections for 852 upper-air sites worldwide are calculated throughout the troposphere and lower stratosphere (up to the altitude of the 5 hPa level). As the bias corrections in the troposphere cannot be calculated using RO Tdry as a reference, a smooth transition to the default bias correction of 0.1 K is applied below the lowest altitude where valid RO Tdry departures are available. Furthermore, within this project, bias corrections for combined SEA ranges were calculated. If the sample size of RS profiles within a specific SEA range is too small to calculate valid statistics, the bias correction for combined SEA ranges is used instead. If insufficient RS profiles are available at a station, a default correction of 0.1 K is applied throughout the whole profile. Thus, a bias correction for all 852 stations separated into four SEA ranges (possibly combined) is calculated. The results are saved in a format which can be used in the forecast impact study.

For the purpose of the calculation of RS biases using RO BAs as an unbiased reference, a cut-off for the BA departures was introduced in Tradowsky [35]. It is essential to calculate the Tdry departures from only a subset of the BA departures, ranging from the lowest dry level of the atmosphere up to the typical burst altitude of RS. Using model information up to a higher level would invalidate the central assumption of the double differencing technique, i.e. the model bias is constant over the separation distance. Though, as every assumption made in a retrieval, choosing an upper cut-off is adding structural uncertainty. This uncertainty is estimated using the range of the Tdry departures calculated for different cut-off impact heights. It is shown that the range of worldwide Tdry departures agrees well with the estimation of the structural uncertainty in different RO retrievals (see e.g Ho et al. [18], Steiner et al. [32]). Furthermore it is shown that applying a cut-off provides similar results as blending the RO and model BA profiles with smooth climatological BA profiles - this is what is typically done in the conventional RO temperature retrieval.

The method used here to calculate RS biases can also be used to compare the temperature departure profiles of the GRUAN reference RS data product with the RO derived Tdry

departures. As both RO and GRUAN are known to be of high quality, good agreement is expected. The GRUAN uncertainty estimate is propagated into the mean GRUAN departure and is shown in the associated uncertainty bars. Two different estimates of the RO uncertainty are presented, i.e. either using entirely the sampling uncertainty or combining the sampling and the structural uncertainty. Consistency and agreement between the RO O-Bs and the GRUAN O-Bs is discussed based on Immler et al. [19] for six GRUAN upper-sir sites, i.e. Lindenberg, Cabauw, Southern Great Plains, Barrow, Ny Ålesund, and Sodankylä. For most GRUAN sites consistency or agreement is found at high, low, and dusk/dawn SEAs at most levels, excluding the 10 hPa level. At the 10 hPa level, the RO O-B minus the GRUAN O-B are negative for high SEA at all sites. This could be caused by a warm temperature bias in the GRUAN data product for the Vaisala RS92 version_2 which is analysed here. A similar results was observed by Ladstädter et al. [24].
At Ny Ålesund and Sodankylä negative double differences are also found for dusk and night SEA at the highest level. Further investigation shows that this warm bias at night-time/dusk mainly occurs in the winter months. Possible reasons for this difference between the GRUAN and RO departure are: (i) preferential sampling of the GRUAN data in certain seasons, (ii) proximity to the polar jet; the central assumption of the double differencing technique could be invalidated if the model bias in proximity to the jet is not constant within 500 km around the GRUAN site, and (iii) a sampling bias caused by the dependence of the burst altitude on atmospheric conditions could explain differences in Sodankylä.
During night-time statistically significant positive double differences (RO O-B minus GRUAN O-B) are found at some stations in the lower stratosphere. The largest differences between the GRUAN and the RO departures are found at the Southern Great Plains site, where the departures are statistically significant different for all levels at night-time. It is currently not clear what is causing these differences.

This study thus provides the basis for a forecast impact study to be performed at the Met Office, compares the GRUAN temperature departures with the RO Tdry departures and discussed the structural uncertainty in the retrieval presented by Tradowsky [35]. It is planned to publish the results of the forecast impact study separately at a later time. At the time the second version of this report is published, a peer-reviewed publication presenting and discussing the method applied here is published, see Tradowsky et al. [36].

7.1 Acknowledgements

This report is prepared in close collaboration with Chris Burrows, whom I can't thank enough for his help throughout the whole project. Furthermore I am very thankful to Sean Healy who supported me with fruitful discussions about the investigation of the upper cut-off. Throughout the whole project I worked in collaboration with Bruce Ingleby, whom I am very thankful for his support in the preparation of the forecast impact study. I would certainly like to thank John Eyre who developed the concept for this research project and discussed the results with me throughout the project. Furthermore I'm very thankful to Ian Culverwell and Greg Bodeker who supported me with discussions about the GRUAN analysis. I also like to express my gratitude towards the ROM SAF who provided the funding for this project and the German Academic Exchange Service who grants my PhD funding (DAAD-Doktorandenstipendium).

Bibliography

[1] Agustí-Panareda, A., Vasiljevic, D., Beljaars, A., Bock, O., Guichard, F., Nuret, M., Garcia-Mendez, A., Andersson, E., Bechtold, P., Fink, A., Hersbach, H., Lafore, J.-P., Ngamini, J.-B., Parker, D. J., Redelsperger, J.-L., and Tompkins, A. M. (2009). Radiosonde humidity bias correction over the West African region for the special AMMA reanalysis at ECMWF. *Quart. J. Roy. Meteor. Soc.*, 135:595–617.

[2] Anthes, R. A. (2011). Exploring Earth's atmosphere with radio occultation: contributions to weather, climate and space weather. *Atmos. Meas. Tech.*, 4:1077–1103.

[3] Auligné, T., McNally, A. P., and Dee, D. P. (2007). Adaptive bias correction for satellite data in a numerical weather prediction system. *Quart. J. Roy. Meteor. Soc.*, 133:631–642.

[4] Bevington, P. R. and Robinson, D. K. (2003). *Data Reduction and Error Analysis for the Physical Sciences*. Mc Graw Hill, 3 edition.

[5] Bodeker, G. E., Bojinski, S., Cimini, D., Dirksen, R. J., Haeffelin, M., Hannigan, J. W., Hurst, D. F., Leblanc, T., Madonna, F., Maturilli, M., Mikalsen, A. C., Philipona, R., Reale, T., Seidel, D. J., Tan, D. G. H., Thorne, P. W., Vömel, H., and Wang, J. (2016). Reference upper-air observations for climate: From concept to reality. *Bulletin of the American Meteorological Society*, 97:123–135.

[6] Burrows, C. P. and Healy, S. B. (2016). Sensitivity of radio occultation-based dry temperature retrievals to upper-level information and its relevance to radiosonde bias corrections. Forecasting Research Technical Report 615, Met Office. Available at `http://www.metoffice.gov.uk/binaries/content/assets/mohippo/pdf/library/frtr_615_2016_2p.pdf`.

[7] Dee, D. P. (2004). Variational bias correction of radiance data in the ECMWF system. ECMWF conference paper, European Centre for Medium-Range Weather Forecasts. Available at `http://www.ecmwf.int/sites/default/files/elibrary/2004/8930-variational-bias-correction-radiance-data-ecmwf-system.pdf`.

[8] Derber, J. C. and Wu, W.-S. (1998). The Use of TOVS Cloud-Cleared Radiances in the NCEP SSI Analysis System. *Mon. Wea. Rev.*, 126:2287–2299.

[9] Dirksen, R. J., Sommer, M., Immler, F. J., Hurst, D. F., Kivi, R., and Vömel, H. (2014). Reference quality upper-air measurements: GRUAN data processing for the Vaisala RS92 radiosonde. *Atmos. Meas. Tech.*, 7:4463–4490.

[10] Eyre, J. R. (1992). A bias correction scheme for simulated TOVS brightness temperatures. ECMWF Technical Memorandum 186, European Centre for Medium-Range Weather Forecasts. Available at `http://www.ecmwf.int/sites/default/files/elibrary/1992/9330-bias-correction-scheme-simulated-tovs-brightness-temperatures.pdf`.

[11] GCOS-112 (2007). GCOS REFERENCE UPPER-AIR NETWORK (GRUAN): Justification, requirements, siting and instrumentation options. Technical Report GCOS-112 (WMO/TD No. 1379), World Meteorological Organization. Available at `https://www.wmo.int/pages/prog/gcos/Publications/gcos-112.pdf`.

[12] Haimberger, L., Tavolato, C., and Sperka, S. (2012). Homogenization of the Global Radiosonde Temperature Dataset through Combined Comparison with Reanalysis Background Series and Neighboring Stations. *J. Climate*, 25:8108–8131.

[13] Hardiman, S. C., Boutle, I. A., Bushell, A. C., Butchart, N., Cullen, M. J. P., Field, P. R., Furtado, K., Manners, J. C., Milton, S. F., Morcrette, C., O'Connor, F. M., Shipway, B. J., Smith, C., Walters, D. N., Willet, M. R., Williams, K. D., Wood, N., Abraham, N. L., Eeble, J. K., Maycock, A. C., Thuburn, J., and Woodhouse, M. T. (2015). Processes controlling tropical tropopause temperature and stratospheric water vapor in climate models. *J. Climate*, 28:6516–6535.

[14] Harris, B. A. and Kelly, G. (2001). A satellite radiance-bias correction scheme for data assimilation. *Quart. J. Roy. Meteor. Soc.*, 127:1453–1468.

[15] He, W., Ho, S.-P., Chen, H., Zhou, X., Hunt, D., and Kuo, Y.-H. (2009). Assessment of radiosonde temperature measurements in the upper troposphere and lower stratosphere using COSMIC radio occultation data. *Geophys. Res. Lett.*, 36.

[16] Healy, S. B. (2008a). Assimilation of GPS Radio Occultation Measurements at ECMWF. In *GRAS SAF Workshop on Applications of GPSRO Measurements, 16-18 June 2008*, pages 99–109, ECMWF, Shinfield Park, Reading, UK. European Centre for Medium-Range Weather Forecasts. Available at `http://www.romsaf.org/Workshops/agrom_prog/Healy.pdf`.

[17] Healy, S. B. (2008b). Forecast impact experiment with a constellation of GPS radio occultation receivers. *Atmos. Sci. Let.*, 9:111–118.

[18] Ho, S.-P., Hunt, D., Steiner, A. K., Mannucci, A. J., Kirchengast, G., Gleisner, H., Heise, S., von Engeln, A., Marquardt, C., Sokolovskiy, S., Schreiner, W., Scherrlin-Pirscher, B., Ao, C., Wickert, J., Syndergaard, S., Lauritsen, K. B., Leroy, S. S., Kursinski, E. R., Kuo, Y.-H., Foelsche, U., Schmidt, T., and Gorbunov, M. (2012). Reproducibility of GPS radio occultation data for climate monitoring: Profile-to-profile inter-comparison of CHAMP climate records 2002 to 2008 from six data centers. *J. Geophys. Res.*, 117.

[19] Immler, F. J., Dykema, J., Gardiner, T., Whiteman, D. N., Thorne, P. W., and Vömel, H. (2010). Reference Quality Upper-Air Measurements: guidance for developing GRUAN data products. *Atmos. Meas. Tech.*, 3(5):1217–1231.

[20] Ingleby, B. and Edwards, D. (2015). Changes to radiosonde reports and their processing for numerical weather prediction. *Atmos. Sci. Let.*, 16:44–49.

[21] Kobayashi, S., Ota, Y., Harada, Y., Ebita, A., Moriya, M., Honoda, H., Onogi, K., Kamahori, H., Kobayashi, C., Endo, H., Miyaoka, K., and Takahashi, K. (2015). The JRA-55 Reanalysis: General Specifications and Basic Characteristics. *J. Meteorol. Soc. Jpn.*, 93:5–48.

[22] Kursinski, E. R., Hajj, G. A., Leroy, S. S., and Herman, B. (2000). The GPS Radio Occultation Technique. *Terrestrial, Atmospheric and Oceanic Sciences*, 11(1):53–114.

[23] Kursinski, E. R., Hajj, G. A., Schofield, J. T., Linfield, R. P., and Hardy, K. R. (1997). Observing Earth's atmosphere with radio occultation measurements using the Global Positioning System. *J. Geophys. Res.*, 102:23429–23465.

[24] Ladstädter, F., Steiner, A. K., Schwärz, M., and Kirchengast, G. (2015). Climate intercomparison of GPS radio occultation, RS90/92 radiosondes and GRUAN from 2002-2013. *Atmos. Meas. Tech.*, 8(3):1819–1834.

[25] Leroy, S. S., Dykema, J. A., and Anderson, J. G. (2006). Climate Benchmarking Using GNSS Occultation. In Foelsche, U., Kirchengast, G., and Steiner, A., editors, *Atmosphere and Climate Studies by Occultation Methods*, pages 287–301. Springer-Verlag.

[26] Milan, M. and Haimberger, L. (2015). Predictors and grouping for bias correction of radiosonde temperature observations. *J. Geophys. Res. Atmos.*, 120:10736–10766.

[27] Poli, P., Healy, S. B., and Dee, D. P. (2010). Assimilation of Global Positioning System radio occultation data in the ECMWF ERA-Interim reanalysis. *Q. J. R. Meteorol. Soc.*, 136:1972–1990.

[28] Rennie, M. P. (2010). The impact of GPS radio occultation assimilation at the Met Office. *Quart. J. Roy. Meteor. Soc.*, 136:116–131.

[29] Rodgers, C. D. (2000). *Inverse Methods for Atmospheric Sounding, Theory and Practice*. World Scientific.

[30] Simmons, A. J., Poli, P., Dee, D. P., Berrisford, P., Hersbach, H., Kobayashi, S., and Peubey, C. (2014). Estimating low-frequency variability and trends in atmospheric temperature using ERA-Interim. *Quart. J. Roy. Meteor. Soc.*, 140:329–353.

[31] Sommer, M., Dirksen, R., and von Rohden, C. (2014). Brief Description of the RS92 GRUAN Data Product (RS92-GDP). GRUAN Technical Document 4, GCOS Reference Upper-Air Network (GRUAN). Version 2.0.3, available at `http://www.dwd.de/EN/research/international_programme/gruan/download/gruan_td-4.pdf?__blob=publicationFile&v=2`.

[32] Steiner, A. K., Hunt, D., Ho, S.-P., Kirchengast, G., Mannucci, A. J., Scherllin-Pirscher, B., Gleisner, H., von Engeln, A., Schmidt, T., Ao, C., Leroy, S. S., Kursinski, E. R., Foelsche, U., Gorbunov, M., Heise, S., Kuo, Y.-H., Lauritsen, K. B., Marquardt, C., Rocken, C., Schreiner, W., Sokolovskiy, S., Syndergaard, S., and Wickert, J. (2013). Quantification of structural uncertainty in climate data records from gps radio occultation. *Atmospheric Chemistry and Physics*, 13(3):1469–1484.

[33] Sun, B., Reale, A., Schroeder, S., Seidel, D. J., and Ballish, B. (2013). Toward improved corrections for radiation-induced biases in radiosonde temperature observations. *J. Geophys. Res.*, 118:4231–4243.

[34] Sun, B., Reale, A., Seidel, D. J., and Hunt, D. C. (2010). Comparing radiosonde and COSMIC atmospheric profile data to quantify differences among radiosonde types and the effects of imperfect collocation on comparison statistics. *J. Geophys. Res.*, 115.

[35] Tradowsky, J. S. (2015). Characterisation of radiosonde temperature biases and errors using radio occultation measurements. ROM SAF Visiting Scientist report 26, Radio Occultation Meteorology Satellite Application Facility. Available at `http://www.romsaf.org/Publications/reports/romsaf_vs26_rep_v12.pdf`.

[36] Tradowsky, J. S., Burrows, C. P., Healy, S. B., and Eyre, J. R. (2017). A new method to correct radiosonde temperature biases using radio occultation data. *Journal of Applied*

Meteorology and Climatology, 56(6):1643–1661. doi:10.1175/JAMC-D-16-0136.1.

[37] Walters, D., Wood, N., Vosper, S., and Milton, S. (2014). ENDGame: A new dynamical core for seamless atmospheric prediction. Met Office Report, Met Office. Available at `http://www.metoffice.gov.uk/media/pdf/s/h/ENDGameGOVSci_v2.0.pdf`.

[38] WMO-No. 306 (2011). Manual on Codes, International Codes, Volume I.2. Technical Report WMO-No. 306, World Meteorological Organization. 2015 edition, available at `http://library.wmo.int/pmb_ged/wmo_306-I2_en.pdf`.

A Acronyms and abbreviations

BA	Bending Angle
CDOP-2	Second Continuous Development and Operations Phase
COSMIC	Constellation Observing System for Meteorology, Ionosphere, and Climate
DMI	Danish Meteorological Institute (ROM SAF Leading Entity)
ECMWF	The European Centre for Medium-Range Weather Forecasts
EPS	EUMETSAT Polar Satellite System
EUMETSAT	European Organisation for the Exploitation of Meteorological Satellites
GCOS	Global Climate Observing System
GNSS	Global Navigation Satellite System
GRAS	GNSS Receiver for Atmospheric Sounding (onboard Metop)
GRUAN	GCOS Reference Upper-Air Network
GDP	GRUAN Data Product
IEEC	Institut d'Estudis Espacials de Catalunya
Met Office	United Kingdom Meteorological Office
Metop	Meteorological Operational Polar satellite (EUMETSAT)
NCEP	National Centers for Environmental Prediction
O-B, OB	Observation minus Background
RO	Radio Occultation
ROM SAF	Radio Occultation Meteorology SAF (former GRAS SAF)
ROPP	Radio Occultation Processing Package
RS	Radiosonde
SAF	Satellite Application Facility (EUMETSAT)
SEA	Solar Elevation Angle
SE	Standard Error
SD	Standard Deviation
Tdry	Dry temperature

B Radiosonde types

Table B.1: *Extract of the radiosonde types used for TEMP reports submitted to the GTS in 2014 (see WMO-No. 306 [38]).*

Number	RS type	Produced in
7	iMet-1-AB	USA
9	No radiosonde - system unknown or not specified	
10	Sippican LMS5	USA
11	Sippican LMS6	USA
14	Vaisala RS92/DigiCORA MW41	Finland
15	PAZA-12M/Radiotheodolite-UL	Ukraine
16	PAZA-22/AVK-1	Ukraine
17	Graw DFM-09	Germany
18	Graw DFM-06	Germany
21	RSG-20A and Jin Yang 1524LA	Korea
22	Meisei RS-11G GPS	Japan
26	Meteolabor SRS-C34/Argus 37	Switzerland
27	AVK-MRZ	Russia
28	AVK -AK2-02	Russia
29	MARL-A and Vektor-M -AK2-02	Russia
30	Meisei RS-06G	Japan
31	Taiyuan GTS1-1/GFE(L)	China
32	Shanghai GTS1-1/GFE(L)	China
33	Nanjing GTS1-2/GFE(L)	China
41	Vaisala RS41 DigiCORA MW41	Finland
49	VIZ MARK II	USA
51	VIZ-B2	USA
52	Vaisala RS92-NGP/Intermet IMS-2000	Finland/USA
55	Meisei RS-01G	Japan
57	Modem M2K2-DC	France
60	MARL-A or Vektor-M - I-2012	Russia
62	MARL-A or Vektor-M - MRZ-3MK	Russia
58	AVK-BAR	Russia
68	AVK-RZM-2	Russia
69	MARL-A or Vektor-M-RZM-2	Russia
71	Vaisala RS90/Loran/Digicora I, II or Marwin	Finland
75	AVK-MRZ-ARMA	Russia
77	Modem GPSsonde M10	France
78	Vaisala RS90/Digicora III	Finland
79	Vaisala RS92/Digicora I, II or Marwin	Finland
80	Vaisala RS92/Digicora III	Finland
81	Vaisala RS92/Autosonde	Finland
82	Lockheed Martin LMS-6	USA
83	Vaisala RS92-D/Intermet IMS 1500	Finland/USA
87	Sippican MARK IIA	USA
88	MARL-A or Vektor-M-MRZ	Russia
89	MARL-A or Vektor-M-BAR	Russia
90	Radiosonde unknown/not specified	
99	Intermet	South Africa